

Gravitational Instabilities in Two-Component Galaxy Disks with Gas Dissipation

Bruce G. Elmegreen

*IBM T. J. Watson Research Center, 1101 Kitchawan Road, Yorktown Heights, New York
10598 USA*

bge@us.ibm.com

ABSTRACT

Growth rates for gravitational instabilities in a thick disk of gas and stars are determined for a turbulent gas that dissipates on the local crossing time. The scale heights are derived from vertical equilibrium. The accuracy of the usual thickness correction, $(1 + kH)^{-1}$, is better than 6% in the growth rate when compared to exact integrations for the gravitational acceleration in the disk. Gas dissipation extends the instability to small scales, removing the minimum Jeans length. This makes infinitesimally thin disks unstable for all Toomre- Q values, and reasonably thick disks stable at high Q primarily because of thickness effects. The conventional gas+star threshold, Q_{tot} , increases from ~ 1 without dissipation to 2 or 3 when dissipation has a rate equal to the crossing rate over a perturbation scale. Observations of $Q_{\text{tot}} \sim 2 - 3$ and the presence of supersonic turbulence suggest that disks are unstable over a wide range of scales. Such instabilities drive spiral structure if there is shear and clumpy structure if shear is weak; they may dominate the generation of turbulence. Feedback regulation of Q_{tot} is complex because the stellar component does not cool; the range of spiral strengths from multiple arm to flocculent galaxies suggests that feedback is weak. Gravitational instabilities may have a connection to star formation even when the star formation rate scales directly with the molecular mass because the instabilities return dispersed gas to molecular clouds and complete the cycle of cloud formation and destruction. The mass flow to dense clouds by instabilities can be 10 times larger than the star formation rate.

Subject headings: Instabilities — Stars: formation — ISM: general — Galaxies: structure

1. Introduction

The stability of a galactic disk with gas and stars was first considered in the context of stellar waves by Lin & Shu (1966) and in the context of cloud formation by Jog & Solomon (1984). The importance of cold gas in the general stability of a combined disk was recognized by Toomre (1964), who also considered the effects of thickness and particle dynamics for the stars, as did Kalnajs (1965). Two-component disks of finite thickness were considered in more detail for the spiral wave problem by Kato (1972) and Bertin & Romeo (1988) and in the general case by Romeo (1992). Rafikov (2001) investigated multiple components.

With these two-component analyses came stability parameters that determined in absolute terms when a disk was stable. For one stellar component, this is the Toomre (1964) value for the minimum velocity dispersion in the radial direction, written now as a dimensionless parameter Q . Goldreich & Lynden-Bell (1965) evaluated a maximum density for the stability of a one-component disk. Following the two-fluid analysis by Jog & Solomon (1984), Elmegreen (1995) and Jog (1996) determined a combined Q for a two-fluid disk. A simpler form for the combined Q was written by Wang & Silk (1994), and recently improved by Romeo & Wiegert (2011). Rafikov (2001) discussed disk stability using the dispersion relation at zero frequency, which is a function of wavenumber, and gave an expression that was compared to observations for spiral galaxies and dwarfs by Leroy et al. (2008). Leroy et al. evaluated the Rafikov expression assuming a range of likely wavenumbers, and showed that most radii in all of the galaxies they studied were marginally stable. This common feature suggests that galaxies regulate their stability by varying the velocity dispersions of gas and stars through star formation feedback and stellar wave scattering.

An important component of disk stability that has been overlooked in these studies is the dissipation of energy in the interstellar medium. Usually the gas is assumed to be isothermal or polytropic, which has a certain level of dissipation by assumption, but the nature of this dissipation is unrealistic as it implies an ever-present source of energy to accompany any decompression. On average, lower-density gas is warmer than higher-density gas, but this relationship is established in the real ISM by specific energy sources and sinks that do not automatically heat up the gas if it is driven to a lower density by gravity. A time-dependent energy equation should be used instead of an adiabatic pressure-density relation. In equilibrium, this energy equation states that heating balances cooling, but out of equilibrium, when a spiral arm or cloud begins to form in an instability, there is usually a net cooling from dissipation in turbulence. Only after the spiral or cloud make stars will the energy loss be returned, but this is long after the instability has grown. Recent computer simulations suggest that the primary role of star formation feedback in a galaxy model is to break apart the dense clouds that form; turbulence on larger scales is driven by gravitational

instabilities (Bournaud et al. 2010, Hopkins et al. 2011, see also Elmegreen et al. 2003). This means that turbulent dissipation accompanies the growth of gravitational instabilities.

The purpose of this paper is to introduce the energy equation to the interstellar component of the stability problem for a gas and star disk. We also consider thickness effects in some detail, checking the approximation often used for stability analyses with an exact integration for the gravitational acceleration in a three dimensional disk. Then we discuss corrections to the commonly used stability thresholds that arise from gaseous energy dissipation. The main point is that energy dissipation changes the dispersion relation for disk instabilities in a fundamental way, removing the Jeans length from the problem in some cases, and giving residual instabilities at high wavenumbers even when the Toomre Q parameters are large. Disk thickness is a more effective stabilizer than interstellar turbulent pressure.

The results have implications for the interpretation of observations, primarily in suggesting a better stability threshold when dissipation is important, and they have implications for simulations of galaxy disks. In simulations, an equation of state for the gas has to be considered to connect density changes with pressure changes. If this equation of state is too simple, particularly if it does not reproduce the expected rapid dissipation of turbulent energy in perturbations, then the simulation is probably more stable than a real galaxy – at least on small scales.

Another application is to regions of galaxies where the usual stability parameters suggest a high degree of stability, such as the far-outer regions of disks, or in dwarf galaxies (Hunter & Plummer 1996; Meurer et al. 1996; van Zee et al. 1997; Hunter et al. 1998). The present results suggest that these regions can still be unstable at a low level as perturbations in density lead to a simultaneous increase in self-gravity and a decrease in gaseous velocity dispersion because of dissipation. Such a region will collapse if dissipation operates on about a crossing time, because the pressure does not increase fast enough to overcome gravity.

In what follows, the star+gas dispersion relation is derived in Section 2, a simple example including turbulent dissipation but without stars is discussed in Section 3, and the star+gas relation is evaluated in Section 4. Gas and star growth rates are considered separately in Section 4.1 and together in Section 4.2. The ratio of perturbed stellar and gaseous column densities is in Section 4.3. Section 4.4 discusses dissipation corrections to the popular gas+star Q thresholds that are in the literature. Section 5 examines thresholds for azimuthal instabilities. A discussion of several implications of this work is in Section 6, including the greater role played by instabilities when dissipation is included (Sect. 6.1), feedback regulation of disk stability (Sect. 6.2), and star formation (Sect. 6.3). A summary is in Section 7.

The scale height of the disk enters the thickness correction factor in the gravitational forcing term. Scale heights are evaluated in a self-consistent way in Appendix A and used for the solutions of the dispersion relation in Section 4. The accuracy of the thickness correction factor is determined in Appendix B.

2. Dispersion Relation

The equations for perturbed radial and azimuthal motions of gas in an axisymmetric galaxy disk are (e.g., Rafikov 2001)

$$\frac{\partial v_{g,r}}{\partial t} - 2\Omega v_{g,\theta} = -\frac{\partial \phi}{\partial r} - \frac{1}{\rho_{g,0}} \frac{\partial P}{\partial r}, \quad (1)$$

$$\frac{\partial v_{g,\theta}}{\partial t} - 2B v_{g,r} = 0. \quad (2)$$

Here, $v_{g,r}$ and $v_{g,\theta}$ are the perturbed radial and azimuthal gas velocities, ϕ is the perturbed gravitational potential, P is the perturbed pressure and $\rho_{g,0}$ is the unperturbed gas density. The angular rotation rate is Ω , and B is the Oort constant of rotation.

Perturbations of the form $e^{i(kr - \omega_i t)}$ are typically introduced. The oscillation frequency is denoted by ω_i to distinguish it from a growth rate ω introduced later, i.e., $\omega = -i\omega_i$. The equations of motion are combined with the definition of the epicyclic frequency, $\kappa^2 = -4\Omega B$, to give

$$v_{g,r} = -\frac{k\omega_i}{\kappa^2 - \omega_i^2} (\phi + P/\rho_{g,0}). \quad (3)$$

The stars were originally treated by Toomre (1964), Kalnajs (1965), and Lin & Shu (1966) using the collisionless Boltzmann equation for the phase-space distribution function. After analogous reduction, the stellar equation becomes (see also Rafikov 2001)

$$v_{s,r} = -\frac{k\omega_i\phi}{\kappa^2 - \omega_i^2} \mathcal{F}(\omega_i/\kappa, [k\sigma_s/\kappa]^2) \quad (4)$$

where

$$\mathcal{F}(s_i, q^2) = \frac{1 - s_i^2}{\sin(\pi s_i)} \int_0^\pi \exp(-q^2[1 + \cos \xi]) \sin(s_i \xi) \sin \xi d\xi \quad (5)$$

(Binney & Tremaine 2008). The notation here is that s_i is the dimensionless oscillation frequency, ω_i/κ , to distinguish it from a dimensionless growth rate, $s = -is_i$, introduced below. The radial velocity dispersion of stars in a presumed Schwarzschild distribution function is σ_s ; we define dimensionless wavenumber $q = k\sigma_s/\kappa$.

The left-hand side of Figure 1 shows $\mathcal{F}(s_i, q^2)$ as a function of dimensionless squared wavenumber q^2 for various dimensionless oscillation frequencies s_i . When s_i is small,

$$\mathcal{F}(s_i, q^2) \approx \frac{1 - s_i^2}{1 - s_i^2 + q^2}. \quad (6)$$

In the figure, the solid lines of various colors are the exact values of \mathcal{F} and the dashed lines with the corresponding colors are the approximate values. Toomre (1964) recognized this similarity for $s_i = 0$. The deviation between the two functions is too small to be seen in most of the figure. A blow-up insert shows how similar the solutions are for $s_i = 0.1$ (green curves), $s_i = 0$ (blue curves), and $s_i = 0.5$ (magenta curves). The similarity between the exact and approximate curves for small s_i means that the instability condition for a collisionless stellar fluid, which is derived from the dispersion relation in the limit when $s_i = 0$, is nearly the same as the instability condition for a fluid having the same velocity dispersion and mass column density. This is why the condition $Q_s = \kappa\sigma_s / (3.36G\Sigma_{s,0}) < 1$ for stars has the constant 3.36 in it, while the condition $Q_g = \kappa\sigma_g / (\pi G\Sigma_{g,0}) < 1$ for gas has the constant π . This constant, 3.35828, is the maximum value of $2\pi\mathcal{F}(0, q^2)/q$ over variations in q .

Equations (3) and (4) contain the radial velocity, gravitational potential, and pressure. The latter two are related to the mass column density. This column density is related to velocity through the continuity equation, which is, for perturbed variables,

$$\omega_i \Sigma_g = kv_{g,r} \Sigma_{g,0}. \quad (7)$$

$$\omega_i \Sigma_s = kv_{s,r} \Sigma_{s,0}. \quad (8)$$

Column density is related to pressure through a time-dependent energy equation. The equation for perturbed energy, when multiplied by $\gamma - 1$ for adiabatic index γ , becomes an equation for perturbed pressure changes:

$$\frac{\partial P}{\partial t} = \left(\frac{\gamma P_0}{\rho_{g,0}} \right) \left(\frac{\partial \rho}{\partial t} \right) + (\gamma - 1) (\Gamma - \Lambda). \quad (9)$$

The perturbed rate of increase of energy per unit volume is Γ and the perturbed rate of decrease from radiative cooling and other effects is Λ . We consider that star formation is mostly triggered by the disk instabilities that we want to study, so that before star formation begins, there is very little perturbation in the heating rate. Perturbed heating might come from background supernovae, for example, and depend on the gas density so that the rate changes when the density changes. However, the heating rate from supernovae depends very weakly on density (as $\rho^{-0.1}$, as may be derived from Cioffi et al. 1988), so we set the perturbed Γ equal to zero. This means that the background turbulent heating rate per unit volume does not increase much as the density increases during the growth of a perturbation.

Cooling comes mostly from shocks in an interstellar medium that is supersonically turbulent. The cooling rate should be larger where the kinetic energy density is larger, which is where the pressure is also larger. To the extent that we can approximate the momentum flux for a supersonically turbulent fluid with the pressure term, P , we can also approximate the dissipation time for the corresponding energy density as some number, δ^{-1} , of crossing times in the perturbed region. This crossing time dependence follows from numerical simulations in Mac Low et al. (1998) and Stone et al. (1998). Because the crossing rate is $\sigma_g k$, we write the dissipation rate as

$$(\gamma - 1)(-\Lambda) = -\delta\sigma_g k P. \quad (10)$$

It is significant that the perturbed cooling rate peaks at the same position as the perturbed pressure, rather than at the position of peak pressure gradient. Then the time dependence of the pressure in equation (9) is in phase with the pressure itself,

$$\frac{\partial P}{\partial t} = \left(\frac{\gamma P_0}{\rho_{g,0}} \right) \left(\frac{\partial \rho}{\partial t} \right) - \delta\sigma_g k P. \quad (11)$$

This phase coherence means that the pressure has a component to the time dependence that is exponential. There are no purely oscillatory solutions as there are for polytropic or isothermal gasses. Thus we need solutions of the form $e^{ikr+\omega t}$ for real ω . We also expect that for self-gravitating media there will be growing (unstable) solutions, in which case $\omega > 0$. Note that the derivation of \mathcal{F} also requires the real part of the growth term to be positive so that an integral converges at negative infinite time (Binney & Tremaine 2008, Appendix 6A). We identify ω as the growth rate of the gas+star gravitational instability.

The reduction factor \mathcal{F} includes solutions where the time dependence is exponential. Substituting is for s_i in equation (5), we obtain for growing perturbations,

$$\mathcal{F}_{\text{growth}}(s, q^2) = \frac{1 + s^2}{\sinh(\pi s)} \int_0^\pi \exp(-q^2[1 + \cos \xi]) \sinh(s\xi) \sin \xi d\xi \quad (12)$$

where s is the dimensionless growth rate, $s = \omega/\kappa$. The right-hand side of Figure 1 shows \mathcal{F} for growing solutions. An excellent approximation is equation (6), which is now written

$$\mathcal{F}_{\text{growth}}(s, q^2) \approx \frac{1 + s^2}{1 + s^2 + q^2}. \quad (13)$$

This approximation, shown by the dashed lines, is closer to the exact growth solution than equation (6) was to the oscillatory solution, equation (5).

The dissipation term in equation (9) has another important effect because it removes the minimum unstable length, or Jeans' length, from the problem for an infinitesimally thin disk. When $\delta \neq 0$, arbitrarily small perturbation lengths can dissipate turbulent energy

and drive an instability. It also removes a stability condition: gas perturbations that always cool are always unstable. Then there is no minimum gas column density for instability, nor is there anything analogous to a Toomre Q condition for an infinitesimally thin disk. Note that zero-order heating and cooling are assumed to be in equilibrium. The turbulent dissipation of zero-order pressure is balanced by energy input from background sources, such as supernovae. But to the extent that perturbed pressures driven by self-gravity always dissipate internal turbulent energy faster than they gain turbulent energy from background sources, there is an instability at all length scales. In practice, that means all length scales where the gas is supersonically turbulent. We return to this point in Section 4 where the effects of disk thickness lead to a stability condition again.

At this point we introduce perturbation variables that clearly indicate their spatial phase dependence. We let perturbed pressure, density, column density and gravitational potential vary as $\cos kr$, and we let both velocities vary as $\sin kr$. All perturbed quantities varying in time as $e^{\omega t}$. It follows that equations (3) and (4) become

$$v_{g,r} = \frac{k\omega}{\kappa^2 + \omega^2} (\phi + P/\rho_{g,0}), \quad (14)$$

$$v_{s,r} = \frac{k\omega\phi}{\kappa^2 + \omega^2} \mathcal{F}_{\text{growth}}(\omega/\kappa, [k\sigma_s/\kappa]^2). \quad (15)$$

The continuity equations are

$$\omega\Sigma_g = -kv_{g,r}\Sigma_{g,0}, \quad (16)$$

$$\omega\Sigma_s = -kv_{s,r}\Sigma_{s,0}. \quad (17)$$

The energy (pressure) equation simplifies to

$$P = \frac{\gamma P_0 \Sigma_g}{\Sigma_{g,0}} \left(\frac{\omega}{\omega + \delta\sigma_g k} \right). \quad (18)$$

Pressure goes to zero as ω goes to zero if $\delta \neq 0$. This is why pressure does not enter the stability condition and why there is no minimum length in the case of turbulent dissipation like that given by equation (10).

The final link is between column density and gravitational potential. This comes from Poisson's equation for the gravitational potential and has no time dependence. The equation is three-dimensional, so the perturbed potential depends on the distribution of perturbed density perpendicular to the plane. This leads to correction factors for the mass column densities if only the two-dimensional forcing is considered. Toomre (1964) used a correction factor of $(1 - e^{-kH})/(kH)$ for a one-component uniform disk between $z = \pm H$, while Vandervoort (1970) used $(1 + kH)^{-1}$ from a more detailed analysis. These two factors are

similar, as is the \mathcal{J} factor in Shu (1968, see Vandervoort 1970). The use of analogous correction factors in the two-component case was discussed by Romeo (1992). He concluded that the correction factors cannot generally be applied independently to each component, but if the vertical distributions are somewhat uncoupled, then that approximation should be all right. In this case the result is a perturbed gravitational potential that depends on the perturbed gaseous and stellar column densities with separate and independent correction factors,

$$\phi = \frac{-2\pi G}{k} \left(\frac{\Sigma_g}{1 + kH_g} + \frac{\Sigma_s}{1 + kH_s} \right). \quad (19)$$

We use this approximation here. In Appendix A, the two scale heights H are evaluated from the equations of vertical equilibrium. In Appendix B, we check the thickness approximation in equation (19) by direct integration over the combined density distribution to determine the gravitational acceleration from a perturbation. The result suggests that the $(1 + kH)^{-1}$ correction factors for column density are too low by $\sim 12\%$ at $kH \sim 1 - 10$, but this is the largest error introduced by the thickness approximation for a wide range of $\Sigma_{g,0}/\Sigma_{s,0}$ and other parameters.

With equations (15), (17), and (19) we can eliminate ϕ and $v_{s,r}$ to get an equation for perturbed Σ_s/Σ_g :

$$\frac{\Sigma_s (1 + kH_g)}{\Sigma_g (1 + kH_s)} = \frac{Y_s}{1 - Y_s}, \quad (20)$$

where

$$Y_s = \frac{2\pi G k \Sigma_{s,0} \mathcal{F}_{\text{growth}}(s, q^2)}{(\omega^2 + \kappa^2) (1 + kH_s)} \quad (21)$$

and $s = \omega/\kappa$, $q = k\sigma_s/\kappa$, as defined above.

Now equations (14), (16), (18), (19), and (20) combine to give the dispersion relation,

$$1 = Y_g + Y_s \quad (22)$$

where

$$Y_g = \frac{2\pi G k \Sigma_{g,0}}{(\omega^2 + \kappa^2 + \sigma_g^2 k^2 \omega / [\omega + \delta\sigma_g k]) (1 + kH_g)}, \quad (23)$$

and the square of the unperturbed gas velocity dispersion is $\sigma_g^2 = \gamma P_0 / \rho_{g,0}$. With dimensionless variables, this dispersion relation is

$$1 = \frac{2qS}{Q_g (1 + s^2 + q^2 S^2 s / [s + \delta q S]) (1 + q\hat{H}_g)} + \frac{2q\mathcal{F}_{\text{growth}}(s, q^2)}{Q_s (1 + s^2) (1 + q\hat{H}_s)}, \quad (24)$$

where $s = \omega/\kappa$, $q = k\sigma_s/\kappa$, $S = \sigma_g/\sigma_s$, $\hat{H}_g = H_g\kappa/\sigma_s$, $\hat{H}_s = H_s\kappa/\sigma_s$, $Q_g = \kappa\sigma_g/(\pi G \Sigma_{g,0})$ and $Q_s = \kappa\sigma_s/(\pi G \Sigma_{s,0})$. This expression is analogous to that in Jog & Solomon (1984), Romeo

(1992) and Rafikov (2001). It differs in our consideration of turbulent gas dissipation and in our use of growth solutions for the reduction factor \mathcal{F} .

In Rafikov (2001), the instability condition for a gas+star fluid was that the right-hand side of equation (24), written with $\delta = 0$ and $H_g = H_s = 0$ in his case, had to exceed 1 in the limit of $s = 0$ for some value of wavenumber q . Stability requires the right hand side to be less than 1 at $s = 0$ for all wavenumbers. If $\delta = 0$, we have these conditions too, because then the gas term varies as $qS/(1 + q^2S^2)$ which has a maximum value of 0.5 at $qS = 1$, and then sufficiently small Q_g makes the right hand side larger than 1. When $\delta \neq 0$, however, the gas term varies directly with q when $s = 0$ and there is no maximum value. The right hand side can exceed 1 for $s = 0$ even for very large Q_g , which is normally stable, if q is large enough. For an infinitesimally thin disk, we need $q > Q_g/2S$ or $k > \kappa^2/(2\pi G\Sigma_{g,0})$ for instability in the pure gas case ($\Sigma_{s,0} = 0$) if there is perturbed gaseous energy dissipation of any magnitude, i.e., $\delta > 0$. This is the same as the instability condition for a infinitesimally thin pressure-less fluid, as derived by Toomre (1964, eqn. 21).

3. Jeans Relation with Dissipation

The role of turbulent dissipation in the standard Jeans analysis can be seen from simpler equations involving only the gas. Equation (22) with the first term on the right is for gas only, but that also contains the effects of rotation and finite thickness. Solutions to this equation will be shown in the next section. An even simpler form is to write it for an infinitesimally thin disk without rotation in the form

$$\omega^2 = 2\pi G\Sigma_g k - \frac{\sigma_g^2 k^2 \omega}{\omega + \delta \sigma_g k}. \quad (25)$$

For the present discussion, we make this equation dimensionless by defining the unit of frequency-squared to be $2\pi G\Sigma k_J$ and the unit of wavenumber-squared to be $k_J^2 = 2\pi G\Sigma_g/\sigma_g^2$; k_J is the conventional Jeans wavenumber. The two-dimensional Jeans equation with this normalization is

$$\omega^2 = k - \frac{k^2 \omega}{\omega + \delta k}. \quad (26)$$

This is a cubic equation,

$$\omega^3 + \omega^2 k \delta + \omega(k^2 - k) - k^2 \delta = 0, \quad (27)$$

that can be solved analytically, although the steps are complicated with terms in δ up to order 6.

Figure 2 shows numerical evaluations of this analytical solution as solid lines for $\delta = 0, 0.5$ and 1 . The usual dispersion relation with a wavenumber limit for growth at $k/k_J = 1$ is reproduced in the case of no dissipation, $\delta = 0$. With dissipation, the instability persists at high wavenumber. The origin of this instability is uncompensated gas cooling on δ^{-1} crossing times, aided by self-gravitational contraction. In other words, turbulent shocks dissipate energy and self-gravity then leads to collapse.

Figure 2 also shows as dashed lines solutions with a dissipation rate proportional to $\delta\sigma_{g,0}k^{1/2}$, which is appropriate for a turbulent gas with a velocity dispersion proportional to the square root of the size: $\sigma_g \propto k^{-1/2}$. There is still instability at high k , but the dissipation rate for each k is lower when there are slower motions at that k , and so the growth rate is lower too. The rest of this paper considers only solutions with σ_g independent of k , but the same shift toward lower growth rate at high k would be present in the full solutions too if σ_g increased with size.

4. Evaluation of the Dispersion Relation

4.1. Gas and Stars Considered Separately

The first term on the right of equation (24), when set equal to 1, is the dispersion relation for pure gas, and the second term is the dispersion relation for pure stars. Combined, they are the dispersion relation for stars+gas. We show each of these in the next 2 figures. The scale heights come from Appendix A.

Figure 3 shows the pure-gas dispersion relation on the left and the pure-star dispersion relation on the right. Both peak at dimensionless wavenumber $q \sim 1-2$ and both have growth rates that increase with decreasing Q . In the case of pure gas, the effect of the dissipation term δqS in equation (24) is to stretch the range of instabilities to larger wavenumber. When $\delta = 0$, the growth rate goes to zero at $q \sim 2$ for $Q_g = 0.5$ and at $q = 3.7$ for $Q_g = 0.3$.

In the case of pure stars (Figure 3 right), the full growth solutions are plotted as solid blue curves. These include the scale height term, $1 + q\hat{H}_s$ with a value of \hat{H}_s that increases from 0.34 at $Q_s = 0.35$ for the top blue curve, to 0.39, 0.49, and 0.58 at $Q_s = 0.4, 0.5,$ and 0.6 for blue curves with decreasing heights. They also include the $\mathcal{F}_{\text{growth}}$ term. For comparison, the dashed green curve has $Q_s = 0.5$ and no scale height term. The growth is then faster because the full stellar column density is used, not the value reduced by $1 + q\hat{H}_s$. For the value of $\hat{H}_s = 0.49$ in this $Q_s = 0.5$ case, $1 + q\hat{H}_s \sim 1.49$ at $q = 1$ near the peak, and this makes the growth rate like the one for a full dispersion relation with $Q_s = 0.5/1.49 = 0.34$ at the same q . Figure 3 includes this case as the top blue curve ($Q_s = 0.35$), for confirmation;

the rest of that blue curve differs from the $Q_s = 0.5$, $\hat{H}_s = 0$ case because the scale height term also has a q dependence. That is, at increasing q , the term $1 + q\hat{H}_s$ becomes larger and the gravitating effective column density, $\Sigma_s/(1 + k\hat{H}_s)$, smaller, making the disk less unstable than the $H_s = 0$ solutions.

In a second comparison, Figure 3 (right, red dotted line) also shows the dispersion relation for $Q_s = 0.5$ and $\hat{H}_s = 0$ in the case where the oscillatory solution for the equations of motion are used, with \mathcal{F} from equation (5). This solution has no physical meaning because at such low Q_s the solutions are unstable and not wave-like, but it does show the difference that comes from using oscillatory solutions for the reduction factor, rather than growth solutions. The oscillatory solutions vary approximately as $\mathcal{F} \sim (1 - s_1^2)/(1 - s_1^2 + q^2)$, which is smaller than the growth solutions which vary as $\mathcal{F}_{\text{growth}} \sim (1 + s^2)/(1 + s^2 + q^2)$. This is why the red dotted line in Figure 3 is lower than the green dashed line for $q > 1$.

Figure 4 shows another case with pure gas, this time for $Q_g > 1$, which is normally stable. Here the destabilizing effect of the dissipation term, δqS , can be seen. The solid blue curves are a sequence of increasing $Q_g = 1, 1.2, \text{ and } 1.4$, from left to right, with dissipation $\delta = 1$. The dashed blue curve is the same as the $Q_g = 1$ curve but with smaller dissipation, $\delta = 0.5$, and so smaller growth rate. The solid red curve has the same $Q_g = 1$ and $\delta = 1$ as the top blue curve, but it has a larger scale height obtained by setting $S = 0.4$ instead of 0.2 in the other curves.

Figure 4 indicates that although the dissipative disk is unstable for some $Q_g > 1$, the growth decreases quickly as Q_g increases. Eventually the disk becomes stable at large enough Q_g if the scale height term is included. Recall in Section 2 we said that infinitesimally thin dissipative disks are unstable for any Q_g as long as $q > Q_g/2S$. With finite thickness, there can be stability at high Q_g . Setting $s = 0$ in equation (24) and using only the first term on the right, which is for gas only, we see that if $2qS / \left(Q_g \left[1 + q\hat{H}_g \right] \right) > 1$, then that equation admits unstable solutions with $s^2 > 0$. This condition rearranges to

$$q > \frac{Q_g}{2S - Q_g \hat{H}_g}. \quad (28)$$

With $\hat{H}_g = 0$ we get $q > Q_g/2S$ again, but with $\hat{H}_g > 0$, we also need $Q_g < 2S/\hat{H}_g$. Unwrapping all the dimensionless variables, this condition is $Q_g < 2^{0.5}$ if $H = \sigma_g^2 / (\pi G \Sigma_{g,0})$ for a one-component dissipative disk.

4.2. Gas and Stars Together

Solutions to the combined gas+star dispersion relation (24) are shown in Figure 5. The standard one-component solutions without thickness corrections ($H_i = 0$) are shown for comparison in the left-hand panel as the multicolored dotted line at small q and s . This line is made from the superposition in different colors of a pure-star solution with $Q_s = 0.9$ and $Q_g = \infty$, a pure-gas solution with $Q_s = \infty$, $Q_g = 0.9$, and $\delta = 0$, and a gas+star solution with gas and stars equivalent, using $Q_s = 1.8$, $Q_g = 1.8$, $\delta = 0$, and $S = 1$. They are expected to have the same dispersion relation and they do. Also shown in the left-hand panel as red curves are two pure-gas solutions ($Q_s = \infty$, $Q_g = 0.9$) with different dissipation rates, $\delta = 0.1$ (lower curve) and $\delta = 0.2$. The extension to high q because of dissipation was also shown in Figures 2-4. The solid blue curves are two gas+star one-component-like cases with $Q_s = 0.9$, $Q_g = 0.9$, $\delta = 0$ and $S = 1$, where in the top curve there are no thickness corrections ($\hat{H}_i = 0$) and in the bottom curve there are. Thickness corrections lower the growth rate by about a factor of 60% in this case, where $\hat{H}_s = \hat{H}_g = 0.44$, because $(1 + q\hat{H}_i)^{-1} = 0.6$ at $q = 1.5$ near the peaks of these curves. Finally, another comparison with two different dissipation rates is shown by the dashed blue lines but now with gas+stars together. Here $Q_s = 1$, $Q_g = 0.5$, and $S = 0.5$ in both cases, while $\delta = 0$ for the bottom curve and $\delta = 0.5$ for the top curve. The extension to high q because of dissipation is present.

A range of values for Q_s and Q_g are shown for the two-component dispersion relation with thickness corrections in the middle panel. The dissipation parameter is fixed at $\delta = 0.5$ and the velocity dispersion ratio is $S = 0.5$. These four parameters all enter into the dispersion equation (24) directly. Also fixed is the ratio of the rotation speed to the stellar dispersion $\hat{v}_{\text{rot}} = \hat{v}_{\text{max}} = 8$, the rotation curve slope $\alpha = 0.4$, and the dark matter to disk ratio, $D = 1$, which enter into the scale height equations (A11) and (A12). The sequence of blue curves with decreasing height has $Q_s = 0.5, 1, 1.5$, and 2 for $Q_g = 1$. The sequence of red curves with decreasing height has $Q_g = 0.5, 1$, and 1.5, with $Q_s = 1$. The overlapping case has a dashed blue and red curve. These two sequences are slightly different. As Q_s increases, the peak in the dispersion relation at $q \sim 1 - 2$ gets less prominent and the dominant part of the curve shifts to the right. All that is left to drive the combined instability at low Q_s is the dissipation in the gas, which extends the instability to high q . On the other hand, as Q_g increases, the peak at $q \sim 1 - 2$ remains and even gets relatively stronger as the stellar instability begins to dominate. In all cases, there is a tail of unstable growth at high q from turbulent dissipation.

The effect of the dissipation term δ is shown as a sequence of blue curves in the right-hand panel of Figure 5, and the effect of the velocity dispersion ratio $S = \sigma_g/\sigma_s$ is shown as a sequence of red curves. For all of these, $Q_s = 1$ and $Q_g = 1$. In addition, $\hat{v}_{\text{rot}} = \hat{v}_{\text{max}} = 8$,

$\alpha = 0.4$, and $D = 1$ (which enter into the scale heights and do not matter much). For the blue curves, $\delta = 0, 0.1, 0.3, 0.5$, and 1 with $S = 0.5$, going from bottom to top, and for the red curves $S = 0.1, 0.2, 0.3, 0.5$, and 1 with $\delta = 0.5$ going from right to left. The overlapping case has a dashed blue and red curve. The effect of increasing dissipation is to increase the growth rate at high q , leaving all else about the same. The effect of increasing the gas velocity dispersion relative to the stars is to decrease the dimensionless wavenumber, i.e., make the unstable wavelength longer. This change is because of the larger gaseous scale height as S increases. Along this sequence of S , the dimensionless scale heights are $(\hat{H}_g, \hat{H}_s) = (0.052, 0.81), (0.10, 0.71), (0.15, 0.65), (0.24, 0.56)$, and $(0.49, 0.49)$, respectively. For the entire sequence of δ in the blue curves, (\hat{H}_g, \hat{H}_s) is the same, $(0.24, 0.56)$.

Low S also makes the gas+star system stable at low q in the right-hand panel of Figure 5. This is because the gas self-gravity term is small for small S at fixed Q_g . Note that the ratio qS/Q_g appears in the first term of equation (24) but S does not appear in the second term. As S decreases, the first term becomes smaller compare to the second. For $Q_s = 1$ in this Figure 5, the second term alone, from stars, is not enough to drive an instability when thickness effects are included. When q is small and S is large, the first term, from gas, adds enough forcing to make the system unstable. But when q is small and S is small, the gas does not contribute enough. Another way to see this is that the ratio qS/Q_g equals $\pi G \Sigma_{g,0} k / \kappa^2$ in physical terms. If S decreases at constant Q_s and Q_g , then $\Sigma_{g,0} / \Sigma_{s,0}$ decreases, so the gas becomes less self-gravitating. (Usually one considers that decreasing S corresponds to colder gas and that seems like it would be more unstable, but that is only for a constant $\Sigma_{g,0}$ and not for a constant Q_g .)

4.3. Ratio of Perturbed Surface Densities

The relative contributions from perturbed stars and gas at the onset of the instability may be determined from the ratio of perturbed surface densities using equation (20), which involves the quantity Y_s . This ratio depends on the wavenumber and growth rate and so depends on the solution to the dispersion relation. In dimensionless terms, Y_s equals the second term on the right of equation (24).

Figure 6 (top) shows Σ_s / Σ_g versus dimensionless wavenumber q for all of the gas+star dispersion relations shown in Figure 5, using the same order of panels, curve colors and curve types (the previous curves for single component solutions are not plotted in Fig. 6). The bottom panels show the surface density ratio normalized to its initial ratio. Generally, the stellar contribution to the instability is proportional to the initial star-to-gas ratio. It is equal to this ratio for $q \leq 1$, and less than it for $q > 1$.

For the fastest growing wavenumber, which is usually larger than $q \sim 1$ (Fig. 5), the ratio of stars to gas in the perturbation can be between 0.5 and 1 times the initial ratio. Figure 7 shows histograms of the normalized ratio of perturbed stars to gas at the wavenumber of peak growth. Each histogram is taken from a series of 800 runs with $Q_s = 0.2, 0.4, 0.6$, up to 4, and $Q_g = 0.1, 0.2, 0.2$, up to 4, and for the cases in this range where there is an instability and where the dimensionless wavenumber of peak growth is less than 40. The dissipation parameter δ increases from top to bottom in the figure. With more dissipation, the peaks in the histograms of the left-hand panels, which are for $S = 1$, shift to the left, which means there is an increasing extension of $\Sigma_s \Sigma_{g,0} / \Sigma_g \Sigma_{s,0}$ to very low values. These changes mean that the contribution from gas is becoming more important as turbulent dissipation increases.

The right-hand side of Figure 7 is for lower relative gas velocity dispersion, $S = 0.2$. Aside from an increase in nearly pure-gas instabilities at $\Sigma_s \Sigma_{g,0} / \Sigma_g \Sigma_{s,0} \sim 0$ with increasing δ , there is not much change in the position of the peak. The lower cutoff to the main peak at $\Sigma_s \Sigma_{g,0} / \Sigma_g \Sigma_{s,0} \sim 0.4$ means that gas contributes less to the instability when S is low than when S is high, even when there is dissipation. The reason for this is that when S is low, the first term on the right in equation (24) is low at fixed Q_g .

To derive the absolute ratio of perturbed stars to gas, we recall that the unperturbed ratio is $\Sigma_{s,0} / \Sigma_{g,0} = Q_g / S Q_s$. Then the absolute ratio is $Q_g / S Q_s$ times the relative ratio in Figure 7. For $S = 0.2$, Figure 7 has a peak at a relative ratio of ~ 0.6 , and so the absolute ratio of perturbation strengths is

$$\frac{\Sigma_s}{\Sigma_g} = \frac{Q_g}{Q_s} \times \frac{0.6}{S} \sim 3 \frac{Q_g}{Q_s}. \quad (29)$$

For $S = 1$ and $\delta = 0$, Figure 7 has a peak near 0.9, so $\Sigma_s / \Sigma_g = \sim 0.9 Q_g / Q_s$. For $S = 1$ and $\delta = 1$, the peak is near 0.6, so $\Sigma_s / \Sigma_g \sim 0.6 Q_g / Q_s$. Generally $Q_g < Q_s$, so the perturbed mass in stars is less than or comparable to the perturbed mass in gas for a wide range of cases. When the Q values are large and the main instability involves strong gas dissipation, the normalized density ratios in Figure 7 are much lower, $\sim 0 - 0.2$, and then the relative contribution from stars is less.

A contribution from stars that is comparable to the contribution from gas in an instability, $\Sigma_s / \Sigma_g \sim 1$, implies that spiral arms which form from the instability contain old disk stars. This is obvious and generally acknowledged for spiral arms. However, the same high fraction of disk stars could also be present in instabilities at the dominant wavenumber that make large globular clouds, as in dwarf galaxies with low shear or in highly unstable clumpy galaxies in the early universe (Elmegreen et al. 2009). The oldest disk stars would be less abundant in these clouds than the youngest disk stars because the stellar velocity dispersion increases with age. Still, stars of intermediate and young age that did not form in the clouds

could have an excess abundance compared to the surrounding disk. According to equation (29), this excess in disk stars approximately equals the excess in gas multiplied by the ratio of Q_g to Q_s .

4.4. Instability Thresholds

The stability threshold is given by the dispersion relation at a growth rate of $s = 0$. In the absence of dissipation ($\delta = 0$) and thickness effects ($\hat{H} = 0$), equation (24) is a sum of two terms, $2qS / (Q_g [1 + q^2 S^2])$ and $2q / (Q_s [1 + q^2])$, considering that equation (13) is a good approximation. Each term has a maximum over variations in q equal to $1/Q$. This is how Wang & Silk (1994) derived an approximate instability threshold for the two-fluid instability:

$$\frac{1}{Q_{\text{tot,WS}}} = \frac{1}{Q_g} + \frac{1}{Q_s} > 1. \quad (30)$$

This threshold has been widely used and is more convenient than the exact Q threshold for these conditions that requires solving a cubic equation (Elmegreen 1995). Extrapolation of this method with thickness corrections might suggest that instability of a more realistic thick disk requires

$$\frac{1}{Q_{\text{tot,WSH}}} = \frac{1}{Q_g(1 + q\hat{H}_g)} + \frac{1}{Q_s(1 + q\hat{H}_s)} > 1. \quad (31)$$

Recently, Romeo & Wiegert (2011) proposed a modified form of the Wang & Silk equation that is more accurate in the standard case ($\delta = 0$),

$$\frac{1}{Q_{\text{tot,RW}}} = \frac{1}{Q_g} + \frac{W}{Q_s} > 1 \text{ if } Q_s > Q_g \quad (32)$$

$$\equiv \frac{W}{Q_g} + \frac{1}{Q_s} > 1 \text{ if } Q_s < Q_g. \quad (33)$$

The weighting function is

$$W(S) = \frac{2S}{1 + S^2}, \quad (34)$$

where S is the ratio of velocity dispersions, σ_g/σ_s . The weighting function allows the gas term in equation (24) to contain S . With thickness effects,

$$\frac{1}{Q_{\text{tot,RWH}}} = \frac{1}{Q_g(1 + q\hat{H}_g)} + \frac{W}{Q_s(1 + q\hat{H}_s)} > 1 \text{ if } Q_s > Q_g \quad (35)$$

$$\equiv \frac{W}{Q_g(1 + q\hat{H}_g)} + \frac{1}{Q_s(1 + q\hat{H}_s)} > 1 \text{ if } Q_s < Q_g. \quad (36)$$

We recall here for convenience that the dimensionless quantity $q\hat{H}$ is identical to the physical quantity kH . We test these approximations by finding their values at the limit where $s = 0$ in equation (24). We also test how well they work when gas dissipation is included.

Figure 8 shows numerous plots of peak growth rate versus $1/Q_{\text{tot}}$. Each panel contains 20 blue curves and 20 red curves. The 20 curves correspond to values of $Q_s = 0.2, 0.4, \dots, 4$, and, within each curve, Q_g varies from 0.1 to 4 in steps of 0.1. Thus each curve is a sequence of decreasing peak growth rates for increasing Q_g . The peak growth rate is evaluated only up to a wavenumber of $q = 40$.

The left-hand panels plot the Wang & Silk parameter on the abscissa, with the blue curves for equation (30) and the red curves for equation (31). The middle column plots the Romeo & Wiegert parameter on the abscissa, again using blue to indicate no thickness terms in that parameter. These two columns use a ratio of dispersions $S = 0.2$, which is typical for spiral galaxies. The right-hand panels consider $S = 1$, for which the Wang & Silk parameter is the same as the Romeo & Wiegert parameter.

Thickness effects are considered in the dispersion relation solutions for all of the curves in the top four rows (even when these effects are ignored in the expression for $1/Q_{\text{tot}}$). What differs in these top four rows is the value of the dissipation parameter, δ . The bottom row solves the dispersion relation (24) without dissipation and without thickness terms, taking $\hat{H}_s = \hat{H}_g = 0$; the red and blue curves are the same then.

In all panels, the threshold of stability occurs where the curves intersect the x-axis, at $s_{\text{peak}} = 0$. Evidently, the stability thresholds given by equations (30)-(33) work well in the situations for which they were designed. For an infinitesimally thin disk with no dissipation and a velocity dispersion ratio of $S = 1$ (bottom right panel), the Wang & Silk formula works perfectly: all the curves intercept the $1/Q_{\text{tot,WS}} = 1$ point at $s_{\text{peak}} = 0$. In this limit, the two fluids act as a single fluid because they have the same velocity dispersion. When $S = 0.2$ at zero thickness and no dissipation (lower left panel), the stability threshold is $1/Q_{\text{tot,WS}} = 1.28$ on average for all intercepts. The Romeo & Wiegert relation works well for both S values in the $\delta = \hat{H} = 0$ limits (i.e., in the bottom middle and bottom right panels).

When thickness effects are considered in equation (24), but still without dissipation (top panels), both the Wang & Silk parameter (red curves: top left and top right panels) and the Romeo & Wiegert parameter (red curves: top middle and top right panels) work well in the sense that they intercept the x -axis at $1/Q_{\text{tot}} \sim 1$. Thus equations (31) and (36) are both reasonable approximations to the stability limit on average.

Dissipation lowers $1/Q_{\text{tot}}$ in all cases. Both the red and blue curves in Figure 8 shift to the left in a sequence of increasing δ going from the top row to the fourth row. With

zero thickness, disks are always unstable for large enough wavenumber when dissipation is included (see discussion after equation 24), but for finite thickness, as in the top four panels of Figure 8, a disk eventually become stable when $1/Q_{\text{tot}}$ is small enough (see discussion after equation 28). The blue curves dive into the abscissa at low $1/Q_{\text{tot,WS}}$ and $Q_{\text{tot,RW}}$ because of this disk stability. The red curves approach the abscissa asymptotically as $1/Q_{\text{tot,WSH}}$ and $1/Q_{\text{tot,RWH}}$ go to zero because q at peak growth gets very large when there is dissipation. Then $(1 + q\hat{H})$ pulls down the $1/Q_{\text{tot}}$ parameters at large Q .

The irregular excursions in the red curves of Figure 8 are because of a rapidly decreasing wavenumber at peak growth for increasing Q at very low Q . Recall that for a one-component instability, $k_{\text{peak}} = \pi G \Sigma / \sigma^2$, or $q_{\text{peak}} = (QS)^{-1}$. This large q at small Q enters into the $(1 + q\hat{H})$ factor, and, this, along with slight variations in \hat{H} , makes the excursions.

Figure 9 shows the average x-axis values where the growth rates in Figure 8 are between 0.03 and 0.3. This is a reasonable range to indicate either absolute stability or slow growth in the cases of asymptotic approach to the abscissa. Blue curves are again for Q_{tot} parameters that ignore thickness and red are for those that include thickness (where all of the dispersion relation solutions include thickness). The open square at $\delta = 0$ is the Wang & Silk equation (30) for $S = 0.2$ and $\hat{H} = 0$ in the dispersion relation; the x-symbol is the Romeo & Wiegert result for $S = 0.2$ and $\hat{H} = 0$, and the open triangle is for both Wang & Silk and Romeo & Wiegert at $S=1$ with $\hat{H} = 0$. Figure 9 confirms the result

$1/Q_{\text{tot}}$ parameters decreases with increasing dissipation: for δ in the range from 0.4 – 1, $Q_{\text{tot,WSH}}$ and $Q_{\text{tot,RWH}}$ should be less than $\sim 1.5 - 2$ for instability when $S = 1$, and they should be less than $\sim 3 - 4$ for instability when $S = 0.2$. If thickness effects are ignored in the stability condition (blue curves), then for this same range of δ , $Q_{\text{tot,WS}} = Q_{\text{tot,RW}} < 0.78 - 0.84$ for instability when $S = 1$, and $Q_{\text{tot,WS}} < 0.70 - 0.74$ and $Q_{\text{tot,RW}} < 0.89 - 0.95$ for instability when $S = 0.2$.

These results indicate that unknown dissipation partly compensates for unknown thickness in the stability condition. That is, Q_{tot} conditions that are evaluated incorrectly without including the thickness terms (blue curves in Figure 9) have a threshold for instability that is still close to 1 when dissipation is important. This compensation has been evident for a long time in simpler derivations where one uses the adiabatic expression for pressure, $P \propto \rho^\gamma$, instead of the perturbed energy equation (11). Denser regions are cooler so $\gamma < 1$. The compilation in Myers (1978) suggests that $\gamma \sim 0.25$ at interstellar densities between 0.1 cm^{-3} and 100 cm^{-3} . This index appears in Q_g as $\gamma^{1/2}$ multiplying the velocity dispersion, σ_g . Thus a version of Q_g with adiabatic cooling and thickness corrections is $\gamma^{1/2} \sigma_g \kappa (1 + kH) / \pi G \Sigma_g$. Since $kH \sim 1$ usually, $\gamma^{1/2} (1 + kH) \sim 1$, indicating that cooling effects offset thickness effects even in a simple derivation.

5. Azimuthal Instabilities

The main result of the previous section is that dissipation promotes gravitational instabilities at high wavenumbers even when a gas+star disk is stable by conventional criteria. Thickness effects ultimately stabilize the disk for high Q_g and Q_s . In the most extreme reduction of this result to a single stability parameter Q_{tot} , we find that both the Wang & Silk (1994) and the Romeo & Wiegert (2011) definitions are reasonably good provided the threshold is raised by a factor of 2 to 3, depending on the relative dissipation rate. For example, if significant energy dissipation in the gas occurs in 2 crossing times over a perturbed wavelength ($\delta = 0.5$), then Q_{tot} including thickness effects has to exceed about 2 for stability, instead of the usual value of 1. This is for radial instabilities.

A higher threshold is also likely for azimuthal instabilities of the swing-amplifier type (Toomre 1981). There is a second instability parameter in that case., i.e., X in the notation of Julian & Toomre (1966) and J in the notation of Lau & Bertin (1978).

The X parameter is defined as

$$X = \frac{\lambda_t}{\lambda_{\text{crit}}} \quad (37)$$

where λ_t is the wavelength of the perturbation in the azimuthal direction and $\lambda_{\text{crit}} = 2\pi/k_{\text{crit}}$ for $k_{\text{crit}} = \kappa^2/(2\pi G\Sigma)$. The wavelength in the azimuthal direction is $2\pi R/m$ for radius R and number m of perturbations in the azimuthal direction. Thus

$$X = \frac{R\kappa^2}{2\pi G\Sigma m} = \frac{\hat{R}Q}{2m} = \frac{Q}{2q_t} \quad (38)$$

where quantities have been normalized in the same way as before: $\hat{R} = R\kappa/\sigma$ and $q_t = k_t\sigma/\kappa$, where $k_t = 2\pi/\lambda_t$.

The J parameter is about the same:

$$J = \left(\frac{m}{R}\right) \left(\frac{2\pi G\Sigma}{\kappa^2}\right) \left(\frac{2\Omega}{\kappa}\right) \left(\left|\frac{d\ln\Omega}{d\ln R}\right|\right)^{1/2} = \frac{1}{X} \left(\frac{2\Omega}{\kappa}\right) \left(\left|\frac{d\ln\Omega}{d\ln R}\right|\right)^{1/2}. \quad (39)$$

The terms in parentheses on the right are of order unity for angular rotation rate $\Omega(R)$. For a flat rotation curve, their product is 1.4.

Toomre (1964) noted that the azimuthal instability in a rotating galaxy has the same size limit as the radial instability, i.e., $\lambda_t < \lambda_{\text{crit}}$, which is the requirement that gravity overcomes the centrifugal force that arises when condensing material spins up by the Coriolis force. This means that instability is favored by small X or large J .

Lau & Bertin (1978) and Bertin et al. (1989) introduced an effective two-dimensional stability parameter

$$\frac{1}{Q_{\text{eff}}^2} = \frac{1}{Q^2} + \frac{J^2 Q^4}{4}. \quad (40)$$

The second term is

$$\frac{J^2 Q^4}{4} = (q_t Q)^2 \left(\frac{2\Omega}{\kappa} \right)^2 \left(\left| \frac{d \ln \Omega}{d \ln R} \right| \right) \sim 2 (q_t Q)^2 \quad (41)$$

where the factor 2 is for a flat rotation curve.

The azimuthal instability is stronger if the azimuthal wavenumber q_t is larger. There is no absolute stability threshold if arbitrarily large q_t (or m) are allowed, because Q_{eff} can always be made less than the threshold value of 1 by large enough q_t . However, at high q_t there is also pressure stabilization for an adiabatic gas undergoing azimuthal instabilities. This is the usual Jeans condition. Without an adiabatic gas, this Jeans condition goes away if turbulent dissipation is fast enough, as shown in previous sections.

Transient growth of shearing spiral waves is still possible. If the dissipation rate is faster than the shear rate, then transient growth can lead to runaway growth. What usually stabilizes the swing amplifier at late times is high pressure at the high wavenumbers that are reached by the swept-back, tightly-wound wavelets. With turbulent dissipation, this gas pressure becomes small. Stabilization at late times then comes from thickness effects rather than pressure. That is, thickness dilutes the gravitational force at high wavenumbers by the factor $(1 + kH)^{-1}$.

6. Discussion

6.1. Pervasive Instabilities

Turbulent dissipation, viscosity, and magnetic fields destabilize galaxy disks. All three either decrease or remove the threshold column density for instability. Dissipation does this by removing the stabilization from turbulent pressure, as shown here, while magnetic fields and viscosity remove the stabilization from Coriolis forces, as shown by Elmegreen (1987) and Kim et al. (2002) for the magnetic case, and by Gammie (1996) for the viscous case. All three processes rely on gas. The effects of dissipation discussed here arise if the gas is not isothermal or simply adiabatic, but satisfies an energy equation with excess dissipation over heating in a perturbed region. The particular form for the dissipation rate assumed here, i.e. proportional to the initial crossing rate in a perturbation, $\delta\sigma_g k$, is appropriate for supersonic turbulence in the general interstellar medium (Mac Low et al. 1998; Stone et al.

1998). This result differs qualitatively from the usual result that cooling makes a gas disk more unstable by lowering Q_g . It also differs from the result that adiabatic gas corresponds to greater instability when the adiabatic index γ is lower.

Our primary concern is the stability of galactic gas. This situation differs from the rotating gas disks studied by Gammie (2001), Rice et al. (2003), Mejía et al. (2005), and others in which gravitational fragmentation occurs if the dissipation time is less than about half the rotation time. These authors assume a constant cooling time τ_c for an energy loss rate U/τ_c with internal energy density U . This would take the place of our term $\Gamma - \Lambda$ in equation (9) and therefore differ from our assumed rate, $\delta\sigma_g kP/(\gamma - 1)$, in equation (10). In our equations, the perturbed cooling time is not constant but scales with the size of the region, $\tau_c \propto 1/k$. The other studies consider instabilities in optically thick, subsonic accretion disks around protostars or active galactic nuclei. In this environment, dissipation is difficult because the radiation cannot easily escape. Dissipation may be aided by convection in the lower layers (Boss 2004), or it may be prevented by slow radiative losses at the disk surface (Cai et al. 2010). Galactic gas, in contrast, is optically thin and supersonic. Dissipation is by random shocks and energy loss is by unblocked radiation from the shock fronts. In our case, small-scale instabilities are possible in the rapidly cooled shocked regions, even if they are smaller than the Jeans length at the initial velocity dispersion.

The present result implies that galaxy disks may be more unstable than previously determined from models or computer simulations with isothermal or adiabatic gas. The effective Q threshold for gas+star radial instabilities increases to ~ 2 if turbulent dissipation takes a few crossing times. This increased Q_{tot} value is comparable to what Leroy et al. (2008) found for most regions of their galaxies, which implies that galactic disks are only marginally stable.

Spiral arms are examples of gravitational instabilities that depend on Q_{tot} . Multiple arm galaxies have what Toomre & Kalnajs (1991) called spiral chaos, with gas+star spiral features of all sizes forming everywhere in the disk and continuously replacing old ones that get sheared away. The gaseous parts of disks can have independent instabilities that make spiral arms in a flocculent pattern of star formation (e.g., Elmegreen et al. 2011). Multiple arm and flocculent structure are instabilities covering a wide range of scales. They should pump turbulent energy into the gas (e.g., Bournaud et al. 2010) and heat the stars (Carlberg & Sellwood 1985; Sellwood 2011). Grand design spirals may be triggered by interactions or bars (Kormendy & Norman 1979) but require a marginally stable disk to amplify these perturbations to large arm/interarm contrasts.

Power spectra of optical light in galaxies, including grand-design galaxies like M81, are continuous power-laws suggesting pervasive instabilities and a cascade of power over a

wide range of scales (Elmegreen et al. 2003, 2006). There is no dominance of structure at the fastest-growing wavelength of an instability. Such lengths are a feature of the linear regime and may appear only in young regions that start fairly smooth. Examples might be expanding shells or spiral arm shocks, which sometimes show a characteristic clump scale (Deharveng et al. 2010; Elmegreen et al. 2006).

6.2. Feedback Regulation of Disk Stability

The observation by Leroy et al. (2008) that $Q_{\text{tot}} \sim 2$ for most galaxy disks in their survey implies some regulatory mechanism. Regulation is usually considered to involve star formation so that low Q_{tot} triggers more star formation, which increases σ_g and Q_{tot} (Goldreich & Lynden-Bell 1965). High Q_{tot} triggers less star formation, causing σ_g to decrease by passive cooling, and lowering Q_{tot} to a more unstable value. Q_{tot} also affects the stellar velocity dispersion because growing instabilities scatter disk stars. The present results detach σ_g from Q_{tot} somewhat, because dissipation also lowers σ_g during the initial growth of the instability. Dissipation and instabilities are not two separate steps in this model.

The variety of spiral arm strengths in galaxies suggests that Q_{tot} is not strongly regulated. The stellar spirals in multiple arm and flocculent galaxies vary in strength, from 50% or stronger surface density modulations in multiple arm galaxies to no perceptible modulations in some flocculent galaxies. Of the 197 flocculent galaxies catalogued by Elmegreen & Elmegreen (1987), 85% have no perceptible long-arm spirals at 2μ in the 2MASS survey (Elmegreen et al. 2011). This result suggests that flocculent galaxies have more stable stellar disks than multiple arm galaxies, which means that not all Q_{tot} values are the same. Similarly, in a sample of 147 Ohio State University Bright Galaxy Survey galaxies less inclined than 65° , the distribution function of spiral arm torques is broad and featureless, spanning a factor of ~ 4 (Buta et al. 2005). Spiral arm morphology and strength are the most direct indicators of Q_{tot} , because these structures are what gas+star instabilities make. Star formation does not have such a clear connection with Q_{tot} .

The composite stability conditions shown in Figure 8 illustrate the conventional notion that instabilities maintain Q_{tot} at a marginally unstable value by stirring the stars and gas. If Q_{tot} is small then the threshold, s_{peak} , is large and stirring is active, which lowers Q_{tot} . Feedback is complex for a gas+star fluid, however, because the stars do not cool. If star formation is active, then cool stars can be added continuously to the stellar population, which is like cooling (Carlberg & Sellwood 1985), but the same instabilities also heat the old stars in proportion. Stronger instabilities heat more old stars and, through cloud formation, produce more cool stars. If heating beats cooling in this proportion, then there would be no

feedback to make the stars cooler if Q_{tot} is too high. If cooling from new stars beats heating, then there would be no feedback to make the stars heat up if Q_{tot} is too low.

Feedback stabilization of Q_{tot} is also complex for a gas+star fluid because the cool young stars have the same velocity dispersion and mass as the gas did before the stars formed. Thus the new, cool stars do not add any extra instability to the combined disk. They remove the ability to dissipate energy however, which is a stabilizing effect.

Persistent heating of old stars by gravitational instabilities requires more and more cool gas to maintain a marginal Q_{tot} if there is regulation. This eventually leads to a gas instability that is decoupled from the star instability, i.e., when $S = \sigma_g/\sigma_s \ll 1$. Then there are two peaks in the dispersion relation, one for stars at low q and another for gas at high q (Jog & Solomon 1984; Romeo 1992). Some flocculent galaxies could be in this regime.

If the stellar Q_s is low, then stellar spirals form readily and the disk cannot be stabilized by extra turbulence following star formation. Feedback comes only from stellar heating in the waves. On the other hand, if Q_s is high, then the combined instability shows up primarily in the gas, producing flocculent spirals and filaments of star formation.

Galactic gas accretion can modify Q_{tot} by adding cold gas, and after star formation, by adding slow-moving stars. Following a sudden influx of gas, Q_{tot} should drop and a period of intense spiral arm or clump formation and star formation should begin. When the gas eventually gets converted to stars, Q_{tot} should increase and the spiral arms weaken. This would be a regulatory process that does not connect Q_{tot} with star formation directly but still keeps Q_{tot} at a more-or-less constant value, particularly if the star formation rate is about equal to the galactic accretion rate on average.

6.3. Star Formation

6.3.1. *Is there a Connection with Galactic-Scale Gravitational Instabilities?*

The direct role of gravitational instabilities in star formation is difficult to observe. According to Leroy et al. (2008), Bigiel et al. (2008) and others, star formation only requires molecular gas, and molecular gas only requires sufficient pressure, most of which comes from the weight of the gas layer in the disk. There is nothing about cloud formation or possible instabilities that induce cloud formation in these conditions. Only pressure determines the abundance of dense, star-forming clouds. Krumholz et al. (2009) and Ostriker et al. (2010) reproduce the observed radial profiles of galaxies using only the constraint that molecular clouds are shielded by atomic gas in some type of equilibrium. It is difficult to see how

galactic-scale gravitational instabilities can influence these results as the instabilities operate on the total gas (and stars) without regard to molecular phase. If gravitational instabilities directly triggered star formation, then the primary scaling law should have a star formation rate that depends on a high power, such as 1.5 or 2, of the total gas column density (e.g., Madore 1977; Li et al. 2005), and this is apparently not observed (however, see Yang et al. 2007; Liu et al. 2011). For a review of star formation processes, see McKee & Ostriker (2007).

Perhaps this disconnection between star formation and gravitational instabilities makes sense in retrospect. If the gas is already highly molecular, then the conversion of a little extra atomic material into molecular material by compression in instabilities will not influence the total molecular mass and star formation rate much, nor will any rearrangement of the existing molecular clouds by the unstable motions. Even cloud collisions during an instability would not affect the star formation rate if the molecular depletion time is as constant as it appears to be Leroy et al. (2008). On the other hand, if the gas is highly atomic, then instabilities could promote molecule formation if the density contrast becomes large. However, on the dominant scale of the gas+star instability, which is σ_s/κ (i.e., $q \sim 1$), and for the dominant growth rate, $\omega \sim \kappa$ (i.e., $s \sim 1$), these instabilities would only increase the density by several exponential growth factors during the available shear time. This is not enough compression to make molecular clouds. Star formation has to occur in the non-linear regime of unstable growth, or independently of this growth, when the gas separates from the stars and collapses into dense molecular clouds by its own gravity (e.g., Kim & Ostriker 2002). The stars that helped start the instability will have moved away in their epicycles after this time, with little long-term excess following the clumped gas. Star formation also occurs after the instability causes contraction in the third dimension, considering that giant molecular clouds (GMCs) are smaller than the scale height. In addition, star formation can occur in pressurized shells and cometary structures that are unrelated to galactic-scale instabilities.

The observation of a linear molecular-cloud star formation law, which suggests a secondary role for galactic-scale gravitational instabilities, combined with the observation of a weakly-varying Q_{tot} , which suggests feedback-regulation of Q_{tot} by gravitational instabilities that may trigger star formation, poses an interesting contradiction. Evidently the role of the these instabilities in star formation is indirect.

One possibility is that gravitational instabilities replenish the self-gravitating molecular gas that gets converted into diffuse gas during the star formation process. This way the molecular gas abundance remains constant on average, and the star formation rate does not scale with the cloud formation rate, but only with the current molecular abundance. An example is provided by the simulations in Bournaud et al. (2010) and Hopkins et al. (2011),

which show gravitational instabilities that form self-gravitating gas from diffuse gas, and star formation that disrupts these gravitating clouds, converting a fraction of their gas back into diffuse form. The conversion rate of diffuse gas into self-gravitating gas by galactic-scale instabilities can be much larger than the conversion rate of self-gravitating gas into stars by local collapse. A simple model for this is discussed in the next sub-section.

6.3.2. A Simple Model of Star Formation with a Role for Gravitational Instabilities

A simple model of star formation illustrates how gravitational instabilities can play an important role in cloud formation, which is cloud re-assembly in this picture, and yet not trigger star formation directly or have a direct connection to the star formation rate. In this model, there are three phases of interstellar matter: self-gravitating clouds in which stars form and which are generally molecular, diffuse molecular clouds in which stars do not form because their density is too low, and diffuse atomic or ionized clouds, which are also too low in density to form stars. If, in a certain region their masses are m_3 , m_2 , and m_1 , respectively, then we can write the equations governing their changes:

$$\frac{dm_3}{dt} = \frac{m_1 + m_2}{T_{\text{GI}}} - \frac{d_3 m_3}{T_{\text{burst}}} - \frac{m_3}{T_{\text{consume}}}, \quad (42)$$

$$\frac{dm_2}{dt} = -\frac{m_2}{T_{\text{GI}}} + \frac{d_2 m_3}{T_{\text{burst}}}, \quad (43)$$

$$\frac{dm_1}{dt} = -\frac{m_1}{T_{\text{GI}}} + \frac{d_1 m_3}{T_{\text{burst}}}. \quad (44)$$

The timescales and terms in these equations are as follows. $T_{\text{GI}} = 1/\omega$ is the timescale for gravitational instabilities studied here. For most cases, this is comparable to the epicyclic time, which means that $s \sim 1$ in the dimensionless notation used above. Then the first equation says that the self-gravitating mass increases on the timescale of the gravitational instability with the mass coming from diffuse gas. That is, gravitational instabilities compress all of the gas into discrete self-gravitating clouds, but the practical effect of this for star formation is to move the diffuse gas that lies between existing GMCs onto those GMCs, and to make new GMCs.

T_{burst} is the duration of a single event of star formation in any one cloud, such as the lifetime of an active OB association. It should be something like 10-20 Myr for a $10^5 M_{\odot}$ cloud. The factor d_3 is the fraction of a self-gravitating cloud that is converted into diffuse gas during each burst; it might be 30% or more, considering disruption of a cluster-forming core and all of the associated ionization. It is not likely to be 100% because dense clouds are mostly pushed to the side by pressures from ionization and stellar winds, into shell-like

and cometary structures, without complete disassociation into atoms. Of this disruption fraction, part of it presumably stays in molecular form but at too low a density to form stars immediately. It could be molecular H_2 without much CO, for example. Many local diffuse clouds are in this state (Spitzer & Jenkins 1975). Rahman et al. (2010) discuss observations of the star formation law with explicit consideration of diffuse molecular gas. It could also be in the form of GMC envelopes that are exposed to background starlight and have high ionization fractions and long magnetic diffusion times (Elmegreen 2007). With this term in equation (42), the self-gravitating mass decreases because of cloud disruption on the timescale of the individual burst.

T_{consume} is the consumption time for self-gravitating gas in general. The consumption time is the total self-gravitating molecular cloud mass in a galaxy divided by the total star formation rate. It is usually measured to be ~ 2 Gyr for main galaxy disks (Leroy et al. 2008; Bigiel et al. 2008). The star formation rate is this last term, m_3/T_{consume} .

There are also parameters in these equations that indicate the fractions of the various phases that convert into other phases. The parameter d_2 is the fraction of the gravitating cloud mass that turns into diffuse molecular gas during a burst, and d_1 is the fraction that turns into diffuse atomic or ionized gas; then $d_1 + d_2 = d_3$.

Equations (42)-(44) can be solved numerically for the time dependence of the three phases, but the result of interest here comes more easily by considering the dominant terms. In equation (42), the last term represents the conversion of gas into stars. Because of the low efficiency of star formation, which means the large value of T_{consume} compared to T_{burst} and T_{GI} , this third term is relatively small. In that case, there is a quasi-equilibrium between the three phases in which the time derivatives are small compared to each separate term involving T_{GI} and T_{burst} . In this equilibrium,

$$m_1 \sim \frac{m_3 T_{\text{GI}}}{T_{\text{burst}}} d_1 \quad ; \quad m_2 \sim \frac{m_3 T_{\text{GI}}}{T_{\text{burst}}} d_2. \quad (45)$$

What we would like is a measure of how active the gravitational instabilities are in rebuilding the clouds that form stars. The building rate is $(m_1 + m_2)/T_{\text{GI}}$, because the instability collects all of the gas and places it in dense clouds, which means it converts the diffuse gas into self-gravitating gas. This building rate should be compared with the star formation rate, which is m_3/T_{consume} . The ratio is

$$\left(\frac{m_1 + m_2}{T_{\text{GI}}} \right) \left(\frac{T_{\text{consume}}}{m_3} \right) = \frac{d_3 T_{\text{consume}}}{T_{\text{burst}}} \quad (46)$$

For $d_3 \sim 0.3$, $T_{\text{consume}} \sim 1$ Gyr, and $T_{\text{burst}} \sim 20$ Myr, the ratio is 15.

The point of this simple model is to show how star formation can happen in self-gravitating clouds at a fixed rate, independent of gravitational instabilities, i.e., without

direct triggering, and yet these instabilities are important in maintaining the cloud population so that this star formation processes can continue. The mass flux into self-gravitating clouds is 15 times the mass flux into stars in this example. In practice, other processes of dense cloud formation, such as shell formation around superbubbles, will combine with gravitational instabilities to return diffuse debris back into self-gravitating clouds.

There are many computer simulations of star formation in galaxy disks that contain the basic elements discussed here, namely gravitational instabilities that drive turbulence and dense cloud formation, star formation in the dense clouds with a certain fixed or density-dependent rate, and dense cloud disruption (e.g., Wada & Norman 2007; Robertson & Kravtsov 2008; Dobbs & Pringle 2009; Baba et al. 2009; Gnedin & Kravtsov 2010; Bournaud et al. 2010; Murante et al. 2010; Gnedin & Kravtsov 2011; Ostriker & Shetty 2011; Tasker & Tan 2009; Tasker 2011). These generally have an equation of state for the gas that includes the heightened instability from dissipation that is discussed in the present paper.

7. Summary

Gravitational instabilities in a gas+star galaxy disk are enhanced when gas dissipation is allowed to occur during the growth of the instability. Then the restoring force from pressure and the velocity dispersion are reduced during the unstable growth. This has the effect of removing the minimum wavelength (the Jeans length) from the problem, and for a thin disk, promoting an unstable condition regardless of Q . For a thick disk, the thickness itself is what limits or prevents instabilities by diluting self-gravity in the in-plane direction compared to the Coriolis force.

This paper derived the dispersion relation for small perturbations in a dissipative gas + stellar disk. The effects of disk thickness were considered in detail, including a self-consistent evaluation of the thicknesses of the two components. Threshold effects for an appropriately defined parameter Q_{tot} were determined and found to differ from the usual results determined without explicit inclusion of dissipation. That is, Q_{tot} has to be a factor of 2 to 3 higher than the usual value of unity before a reasonably thick disk becomes significantly stable. This change implies that real galaxy disks are more unstable than previously believed.

The greater instability has implications for spiral waves and cloud formation, and for feedback control of Q_{tot} , which is much more complicated for a two-component disk than a one-component disk, considering that an existing stellar component can never cool. The instability also has implications for star formation laws, particularly if they suggest a linear dependence between the star formation rate and the molecular abundance. Such laws would

not seem to have a role for gravitational instabilities in directly triggering star formation, but they may still have a role in re-assembling the self-gravitating clouds that are torn apart by stellar feedback. The mass exchange in this assembly phase can exceed the mass flow into stars by a factor of 10 or more, indicating the importance of the instability as a component of the whole process.

REFERENCES

- Baba, J., Asaki, Y., Makino, J., Miyoshi, M., Saitoh, T.R., & Wada, K. 2009, *ApJ*, 706, 471
- Bertin, G., & Romeo, A. B. 1988, *A&A*, 195, 105
- Bertin, G., Lin, C.C., Lowe, S.A., & Thurstans, R.P. 1989, *ApJ*, 338, 104
- Bertin, G., & Romeo, A.B. 1988, *A&A*, 195, 105
- Bigiel, F., Leroy, A., Walter, F., Brinks, E., de Blok, W. J. G., Madore, B., & Thornley, M. D. 2008, *AJ*, 136, 2846
- Binney, J., & Tremaine, S. 2008, *Galactic Dynamics*, Princeton University Press
- Boss, A.P. 2004, *ApJ*, 610, 456
- Bournaud, F., Elmegreen, B.G., Teyssier, R., Block, D.L., & Puerari, I. 2010, *MNRAS*, 409, 1088
- Burstein, D., & Rubin, V.C. 1985, *ApJ*, 297, 423
- Buta, R., Vasylyev, S., Salo, H., & Laurikainen, E. 2005, *AJ*, 130, 506
- Cai, K., Pickett, M.K., Durisen, R.H., & Milne, A.M. 2010, *ApJ*, 716, L176
- Carlberg, R. G. & Sellwood, J. A. 1985, *ApJ*, 292, 79
- Cioffi, D.F., McKee, C.F. & Bertschinger, E. 1988, *ApJ*, 334, 252
- Deharveng, L., Schuller, F., Anderson, L. D., Zavagno, A., Wyrowski, F., Menten, K. M., Bronfman, L., Testi, L., Walmsley, C. M., & Wienen, M. 2010, *A&A*, 523, 6
- Dobbs, C. L., & Pringle, J. E. 2009, *MNRAS*, 396, 1579
- Elmegreen, B.G. 1987, *ApJ*, 312, 626
- Elmegreen, B.G. 1995, *ApJ*, 275, 944

- Elmegreen, D.M., & Elmegreen, B.G. 1987, ApJ, 314, 3
- Elmegreen, B.G., Elmegreen, D.M., & Leitner, S. 2003, ApJ, 590, 271
- Elmegreen, B.G., Elmegreen, D.M., Chandar, R., Whitmore, B., & Regan, M. 2006, ApJ, 644, 879
- Elmegreen, D.M., Elmegreen, B.G., Kaufman, M., Sheth, K., Struck, C., Thomasson, M., Brinks, E. 2006, ApJ, 642, 158
- Elmegreen, D.M., Elmegreen, B.G., Marcus, M., Shahinyan, K., Yau, M., & Petersen, M. 2009, ApJ, 701, 306
- Elmegreen, D.M. et al. 2011, in preparation
- Gammie, C.F. 1996, ApJ, 462, 725
- Gammie, C.F. 2001, ApJ, 553, 174
- Goldreich, P. & Lynden-Bell, D. 1965, MNRAS, 130, 97
- Gnedin, N.Y., & Kravtsov, A.V. 2010, ApJ, 714, 287
- Gnedin, N.Y., & Kravtsov, A.V. 2011, ApJ, 728, 88
- Jog, C.J., & Solomon, P.M. 1984, 276, 114
- Jog, C.J. 1996, MNRAS, 278, 209
- Julian, W.H. & Toomre, A. 1966, ApJ, 146, 810
- Hopkins, P.F., Quataert, E., & Murray, N. 2011, arXiv1101.4940
- Hunter, D.A., & Plummer, J.D. 1996, ApJ, 462, 732
- Hunter, D.A., Elmegreen, B.G., & Baker, A.L. 1998, ApJ, 493, 595
- Kalnajns, A.J. 1965, PhD dissertation, Department of Astronomy, Harvard University.
- Kato, S. 1972, PASJ, 24, 61
- Kim, W.-T., & Ostriker, E. C. 2000, ApJ, 540, 372
- Kim, W.-T., Ostriker, E.C., & Stone, J.M. 2002, ApJ, 581, 1080
- Kim, W.-T., & Ostriker, E.C. 2002, ApJ, 570, 132

- Kormendy, J., & Norman, C.A. 1979, *ApJ*, 233, 539
- Krumholz, M. R., McKee, C. F., & Tumlinson, J. 2009b, *ApJ*, 699, 850
- Lau, Y.Y., & Bertin, G. 1978, *ApJ*, 226, 508
- Leroy, A.K., Walter, F., Brinks, E., Bigiel, F., de Blok, W. J. G., Madore, B., & Thornley, M. D. 2008, *AJ*, 136, 2782
- Li, Y., Mac Low, M.-M., & Klessen, R.S. 2005, *ApJ*, 620, L19
- Lin, C. C., & Shu, F.H. 1966, *PNAS*, 55, 229
- Liu, G., Koda, J., Calzetti, D., Fukuhara, M., & Momose, R. 2011, *AAS*, 217, 246.04
- Mac Low, M.-M., Klessen, R.S., Burkert, A., & Smith, M.D. 1998, *PhRvL*, 80, 2754
- Madore, B.F. 1977, *MNRAS*, 178, 1
- McKee, C. F., & Ostriker, E. C. 2007, *ARA&A*, 45, 565
- Mejía, A. C., Durisen, R. H., Pickett, M. K., & Cai, K. 2005, *ApJ*, 619, 1098
- Meurer, G. R., Carignan, C., Beaulieu, S. F., & Freeman, K. C. 1996, *AJ*, 111, 1551
- Murante, G., Monaco, P., Giovalli, M., Borgani, S., & Diaferio, A. 2010, *MNRAS*, 405, 1491
- Myers, P. C. 1978, *ApJ*, 225, 380
- Narayan, C.A., & Jog, C.J. 2002, *A&A*, 394, 89
- Ostriker, E.C., McKee, C.F., & Leroy, A.K. 2010, *ApJ*, 721, 975
- Ostriker, E.C., & Shetty, R. 2011 [arXiv:1102.1446](https://arxiv.org/abs/1102.1446)
- Rafikov, R.R. 2001, *MNRAS*, 323, 445
- Rahman, N., et al. 2010, [arXiv:1009.3272](https://arxiv.org/abs/1009.3272)
- Rice, W. K. M., Armitage, P. J., Bate, M. R., & Bonnell, I. A. 2003, *MNRAS*, 339, 1025
- Robertson, B.E., & Kravtsov, A.V. 2008, *ApJ*, 680, 1083
- Romeo, A.B. 1992, *MNRAS*, 256, 307
- Romeo, A.B., & Wiegert, J. 2011, [arXiv1101.4519](https://arxiv.org/abs/1101.4519)

- Sellwood, J.A. 2011, MNRAS, 410, 1637
- Spitzer, L., Jr., & Jenkins, E. B.1975, ARA&A, 13, 133
- Stone, J. M., Ostriker, E. C., & Gammie, C. F. 1998, ApJ, 508, L99
- Shu, F.H. 1968, PhD Dissertation, Harvard University
- Tasker, E.J., & Tan, J.C. 2009, ApJ, 700, 358
- Tasker, E.J. 2011, ApJ, 730, 11
- Toomre, A. 1964, ApJ, 139, 1217
- Toomre, A. 1981, in The structure and evolution of normal galaxies, Cambridge: Cambridge University Press, p. 111
- Toomre, A., & Kalnajs, A. J. 1991, in Dynamics of Disc Galaxies: Varberg Castle Sweden, p. 341
- Vandervoort, P.O. 1970, ApJ, 161, 87
- van Zee, L., Haynes, M.P., Salzer, J.J., & Broeils, A.H. 1997, AJ, 113, 1618
- Wada, K., & Norman, C.A. 2007, ApJ, 660, 276
- Wang, B., & Silk, J. 1994, ApJ, 427, 759
- Yang, C.-C., Gruendl, R.A., Chu, Y.-H., Mac Low, M.-M., & Fukui, Y. 2007, ApJ, 671, 374

A. Scale Heights

The vertical profiles for perturbed gas and stars in our model are the same as the vertical profiles for equilibrium gas and stars because all of the motions are assumed to be parallel to the disk plane. The scale heights then come from the equations of vertical equilibrium. We follow Narayan & Jog (2002) and write the equation for density of each component $i = g$ and s :

$$\frac{d^2\rho_i}{dz^2} = \frac{\rho_i}{\sigma_i^2} \left(-4\pi G(\rho_g + \rho_s) + \frac{dK_{\text{DM}}}{dz} \right) + \frac{1}{\rho_i} \left(\frac{d\rho_i}{dz} \right)^2, \quad (\text{A1})$$

where the dark matter acceleration per unit length is

$$\frac{dK_{\text{DM}}}{dz} = -\frac{v_{\text{max}}^2}{r^2} \left(1 - \frac{2z^2}{r^2} - \frac{z^2 R_c^2}{r^2(R_c^2 + r^2)} + \left[\frac{R_c}{r} \right] \left[\frac{3z^2}{r^2} - 1 \right] \arctan[r/R_c] \right) \quad (\text{A2})$$

for a dark matter density distribution

$$\rho_{\text{DM}}(r) = \frac{\rho_{\text{DM0}} R_c^2}{R_c^2 + r^2} \equiv \frac{v_{\text{max}}^2}{4\pi G(R_c^2 + r^2)}, \quad (\text{A3})$$

with central density ρ_{DM0} , core radius R_c , 3D radius $r = (R^2 + z^2)^{1/2}$, disk radius in cylindrical coordinates R , and extrapolated rotation speed at infinity, v_{max} .

The rotation curve enters into our primary variable κ , which is used for normalization, so we should be self-consistent in the definitions of these quantities. We write the rotation curve in the midplane as the sum of contributions from the dark matter and the disk,

$$v_{\text{rot}}^2(R) = v_{\text{rot,DM}}^2(R) + v_{\text{rot,Disk}}^2(R) \quad (\text{A4})$$

with

$$v_{\text{rot,DM}}^2(R) = \frac{GM_{\text{DM}}(R)}{R} \quad (\text{A5})$$

and

$$M_{\text{DM}}(R) = \int_0^R 4\pi R^2 \rho_{\text{DM}} dR = 4\pi \rho_{\text{DM0}} R_c^3 \left(\frac{R}{R_c} - \arctan \frac{R}{R_c} \right). \quad (\text{A6})$$

We assume that the disk mass column density profiles are exponential, $\Sigma_{i,0} = \Sigma_{i,00} e^{-R/R_D}$, and have the same disk scale lengths R_D for gas and stars. Then

$$v_{\text{rot,Disk}}^2(R) = 4\pi G (\Sigma_{g,0} + \Sigma_{s,0}) R_D y^2 (I_0[y] K_0[y] - I_1[y] K_1[y]) \quad (\text{A7})$$

in the notation of Binney & Tremaine (2008, eqn. 2.165), with modified Bessel functions I and K , and $y = R/2R_D$.

Note that as $R \rightarrow \infty$, $v_{\text{rot}}^2 \rightarrow 4\pi G \rho_{\text{DM0}} R_c^2$, which is v_{max}^2 in equation (A3). Now we write

$$\kappa^2 = 2 \left(\frac{v_{\text{rot}}}{R} \right)^2 \left(1 + \frac{d \log v_{\text{rot}}}{d \log R} \right) \quad (\text{A8})$$

and define $\alpha = d \log v_{\text{rot}} / d \log R$. This gives a relation between the dimensionless disk radius \hat{R} and the dimensionless rotation speed,

$$\hat{R}^2 = 2(1 + \alpha) \hat{v}_{\text{rot}}^2. \quad (\text{A9})$$

The other dimensionless parameters are related also. From equation (A3), the ratio of the dark matter central column density to the stellar disk central column density is $\pi\rho_{\text{DM}0}R_c/\Sigma_{\text{s},00}$. If we let $D = \rho_{\text{DM}0}R_c/\Sigma_{\text{s},00}$, then

$$\hat{R}_c = \frac{\hat{v}_{\text{max}}^2 Q_s}{4D}. \quad (\text{A10})$$

In terms of the characteristic dimensions used for section 2, namely κ for inverse time and σ_s for velocity, the vertical equilibrium equations in dimensionless form become

$$\frac{d^2 \hat{\rho}_g}{d\hat{z}^2} = \frac{\hat{\rho}_g}{S^2} \left(-\frac{2}{Q_s}(\hat{\rho}_g + \hat{\rho}_s) + \frac{d\hat{K}_{\text{DM}}}{d\hat{z}} \right) + \frac{1}{\hat{\rho}_g} \left(\frac{d\hat{\rho}_g}{d\hat{z}} \right)^2. \quad (\text{A11})$$

$$\frac{d^2 \hat{\rho}_s}{d\hat{z}^2} = \hat{\rho}_g \left(-\frac{2}{Q_s}(\hat{\rho}_g + \hat{\rho}_s) + \frac{d\hat{K}_{\text{DM}}}{d\hat{z}} \right) + \frac{1}{\hat{\rho}_s} \left(\frac{d\hat{\rho}_s}{d\hat{z}} \right)^2. \quad (\text{A12})$$

Equation (A2) for dK_{DM}/dz looks essentially the same in dimensionless form with dimensionless distances like $\hat{r} = r\kappa/\sigma_s$ substituted for physical distances, and with the dimensionless rotation speed $\hat{v}_{\text{rot}} = v_{\text{rot}}/\sigma_s$. In equations (A11) and (A12), dimensionless density is related to physical density as $\hat{\rho} = 2\pi G\rho Q_s/\kappa^2$. Note that for a single fluid, the solution to equation (A11) would be $\hat{\rho}(\hat{z}) = \hat{\rho}(\hat{z} = 0)\text{sech}^2(\hat{z}/\hat{H})$ and the dimensionless scale height would be $\hat{H} = S(Q_s/\hat{\rho}[\hat{z} = 0])^{1/2}$. The dimensionless column density would be $\hat{\Sigma}_0 = \int_{-\infty}^{\infty} \hat{\rho} d\hat{z} = 2\hat{\rho}(\hat{z} = 0)\hat{H}$. For a single fluid in physical units, $H = \sigma^2/(\pi G\Sigma_0) = \sigma/(2\pi G\rho[z = 0])^{1/2}$.

The vertical equilibrium equations may be solved for $\rho_i(z)$ and the scale heights defined as $H_i = 0.5\Sigma_{i,0}/\rho_i(z = 0)$. For the dimensionless solutions, the dimensionless input parameters are Q_s , $S = \sigma_g/\sigma_s$, \hat{v}_{rot} , \hat{v}_{max} , and the dark matter-to-disk column density ratio, D . Also entering is the logarithmic gradient of the rotation curve, α , which varies with radius and depends on D , and disk-to-halo size ratio, R_D/R_c . The unperturbed gas-to-star column density ratio, $\Sigma_{\text{g},0}/\Sigma_{\text{s},0}$ may be treated either as an independent variable, or it can be taken equal to SQ_s/Q_g if Q_g is independently specified.

In practice, we do not need a detailed model of a galaxy just to get an estimate of the scale heights. To simplify things, representative values of α were determined from the average over a range of parameters: $D = (0, 2)$, $\Sigma_{\text{g},0}/\Sigma_{\text{s},0} = (0, 2)$, and $R_D/R_c = (0.2, 2)$. The average α for disk position $R/R_c = 1$ was found to be 0.4, meaning the rotation curve is on the rising part there, and the average for $R/R_c = 4$ is 0.04, which is on the flat part. We consider these two cases in what follows. The first case can apply to both the inner regions of massive disk galaxies and to most of the visible parts of the disks of dwarf galaxies (e.g., Burstein & Rubin 1985).

Figure 10 shows the profiles of $\rho_g(z)$ and $\rho_s(z)$ for several dark matter ratios D and velocity dispersion ratios S . The solid curves are for $\alpha = 0.4$ and the dashed curves for

$\alpha = 0.04$; they hardly differ from each other. For all colors and line types, the lower curves are for gas and the upper curves for stars. When $S = \sigma_g/\sigma_s = 1$ (blue curves), the gas scale height is the same as the stellar scale height and the profiles differ only in amplitude by the ratio of column densities ($\Sigma_{g,0}/\Sigma_{s,0} = 0.2$). When S is small, the gas disk is thin and the dark matter ratio does not affect the gas scale height (red and green curves for gas are about the same). The stellar profile does not depend much on S (blue and green curves for stars are about the same), but it does depend on the dark matter ratio in the sense that less dark matter makes the stellar disk thicker (red curve for stars is higher than the blue or green curves). In all cases, $Q_s = 2$, $\hat{v}_{\text{rot}} = \hat{v}_{\text{max}} = 8$, and $\Sigma_{g,0}/\Sigma_{s,0} = 0.2$.

Figure 11 shows the dimensionless scale heights versus the gas fraction in the disk, $\Sigma_{g,0}/\Sigma_{s,0}$, on the left, versus the velocity dispersion ratio S in the middle, and versus Q_s on the right. These are the parameters that cause the scale heights to vary most. In all cases, $\hat{v}_{\text{rot}} = \hat{v}_{\text{max}} = 8$, and $\alpha = 0.4$. Equations (A11) and (A12) show why the gas scale height increases with S and both scale heights increase with Q_s for this normalization. In the left and middle panels, $Q_s = 2$. Both dimensionless scale heights decrease with increasing $\Sigma_{g,0}/\Sigma_{s,0}$ because then the gas density increases at fixed $\Sigma_{s,0}$ and this pulls in the star layer. Analogous results for $\alpha = 0.04$ and for a wide range of \hat{v}_{rot} are nearly identical to those in Figure 11.

Representative values for normal spiral galaxy disks in the local universe, where $S \sim 0.2 - 0.4$, and $\Sigma_{g,0}/\Sigma_{s,0} \sim 0.2$, are $\hat{H}_g \sim 0.3$ and $\hat{H}_s \sim 1.3$. For clumpy galaxies at high redshift and local dwarfs, $S \sim 0.8 - 1$, and $\Sigma_{g,0}/\Sigma_{s,0} \sim 1$, so $\hat{H}_g \sim 0.7$ and $\hat{H}_s \sim 0.9$. The ratio of the rotation speed to the velocity dispersion of the stars, the slope of the rotation curve, and the ratio of the dark matter to the disk mass do not influence these normalized scale heights significantly.

B. Thickness Correction Factors

Equation (19) contains an approximation for disk thickness that can be evaluated using the full solutions for the vertical density profiles just calculated. If $\rho(z) = \rho_g(z) + \rho_s(z)$ is the vertical distribution of total density in a plane-parallel layer, and if this total density has a $\cos(kx)$ dependence in the direction of the perturbation, as assumed above, then the acceleration measured at position x_0 in the midplane in this direction is

$$g(x_0) = 2G \int_{-\infty}^{\infty} dz \int_{-\infty}^{\infty} dx \frac{\rho(z) \cos(kx)(x - x_0)}{z^2 + (x - x_0)^2}. \quad (\text{B1})$$

This comes from the acceleration $2G\mu/r$ toward a line of mass with mass μ per unit length $\mu = \rho dx dz$ measured at a distance $r = (z^2 + [x - x_0]^2)^{1/2}$. Converting equation (B1) to

dimensionless units as above, separating the gaseous and stellar parts of ρ , setting $g = -d\phi/dx$, and using an equation like (19) with arbitrary correction factors C instead of $(1 + kH)^{-1}$, we get

$$\frac{C_g \Sigma_g}{\Sigma_s} + C_s = \frac{-1}{\pi \sin(qx_0)} \int_0^\infty d\hat{z} \int_{-\infty}^\infty d\hat{x} \frac{\hat{\rho}(\hat{z}) \cos q\hat{x}(\hat{x} - \hat{x}_0)}{\hat{z}^2 + (\hat{x} - \hat{x}_0)^2}. \quad (\text{B2})$$

Note that the cosine term inside the integral gets converted to a sine term after integration, and this phase dependence is divided out by the sine in the denominator. This is consistent with the fact that a cosine variation in density produces a sine variation in gravitational acceleration, and this produces a cosine variation in the potential, which is used in equation (19). The integral was evaluated for a variety of cases over the range $q = (0, 20)$ and the coefficients $C_i = (1 + q\hat{H}_i)^{-1}$ were found to be good approximations.

Figure 12 shows the ratio of the right hand side of equation (B2) to the left hand side using $C_i = (1 + q\hat{H}_i)^{-1}$, plotted as a function of dimensionless wavenumber q . This ratio is the correction factor that should be applied to the right-hand side of equation (19), or to the column densities, to make the thickness correction more accurate when the approximation $(1 + kH)^{-1}$ is used. Alternatively, the inverse of this correction factor can be applied to the stability parameter Q to get a more accurate stability parameter. Fortunately, the correction factor is small, less than 15% in all cases, and only that large near $kH \sim 1 - 4$. In the range $kH \sim 1 - 10$, the average correction in Figure 12 is 12%, which means that the true acceleration that drives the instability is higher than the estimate using the potential of equation (19) by an average of $\sim 12\%$. The instability growth rate scales as the square root of the acceleration per unit length, so the likely correction to the growth rate is an increase by $\sim 6\%$. Considering the other approximations used here for interstellar and stellar dynamics, this correction to the growth rate is not important. We therefore evaluate the dispersion relation using the original Vandervoort approximation, as given by equation (19).

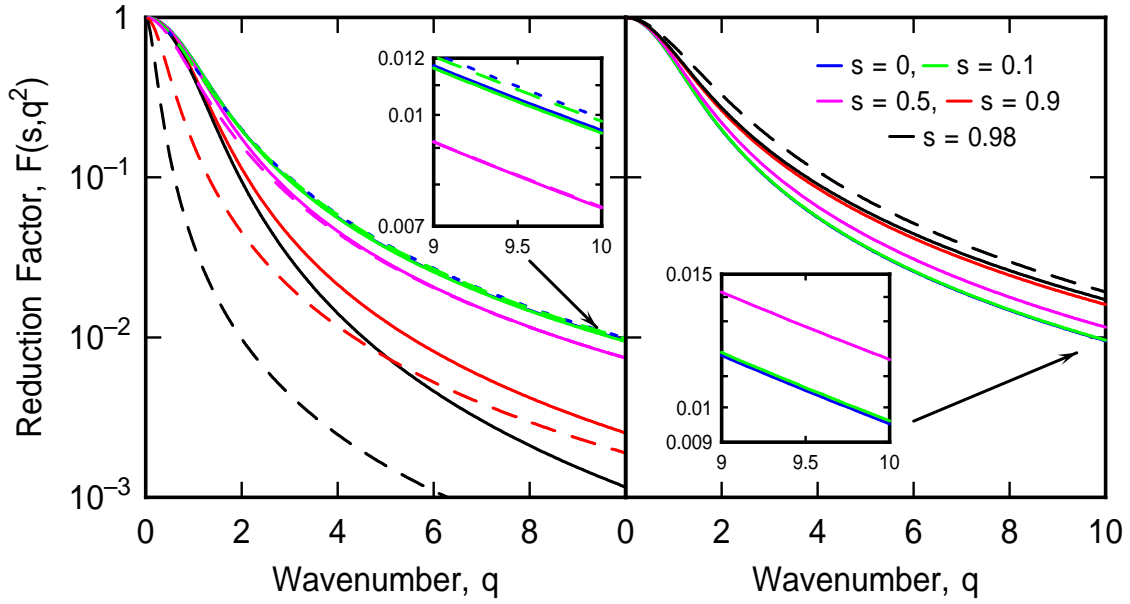


Fig. 1.— The reduction factor \mathcal{F} for gravitational force is plotted versus the dimensionless wavenumber, q , for five different dimensionless rates, s , indicated by color. Oscillating solutions are shown on the left and growing solutions are shown on the right. Dashed lines are approximate solutions from equations (6) and (13).

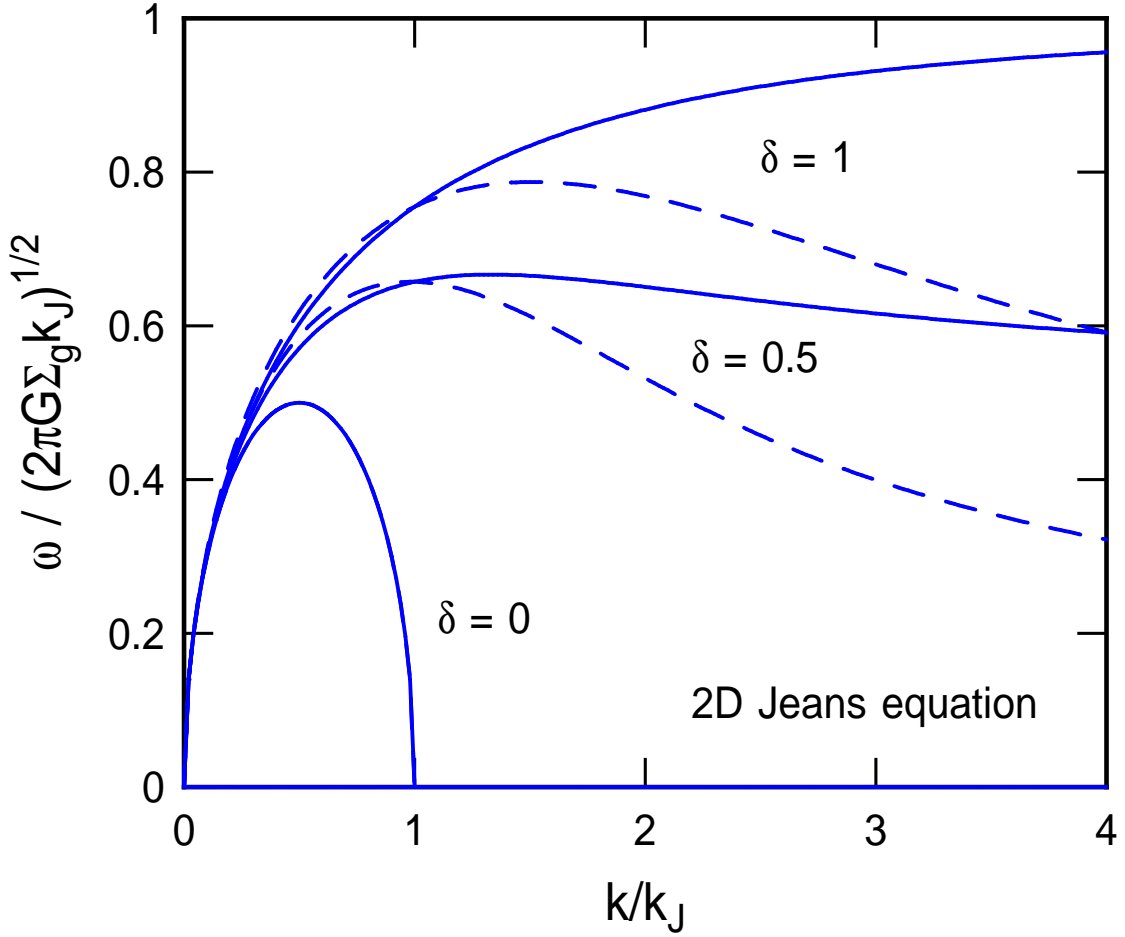


Fig. 2.— Dispersion relation for the planar disk instability with only gas and no rotation, showing the effect of turbulent dissipation. δ is the relative energy dissipation rate compared to the perturbation crossing rate. Without turbulent dissipation ($\delta = 0$), the dispersion relation has the usual upper limit for instability at the Jeans wavenumber $k = k_J$. With turbulent dissipation, the instability also happens in smaller regions because shocks remove energy and promote local gravitational instabilities. Solid lines are for a velocity dispersion that is independent of the size of the perturbation, as in the rest of this paper, and dashed lines are for a velocity dispersion that increases as the square root of the size of the perturbation.

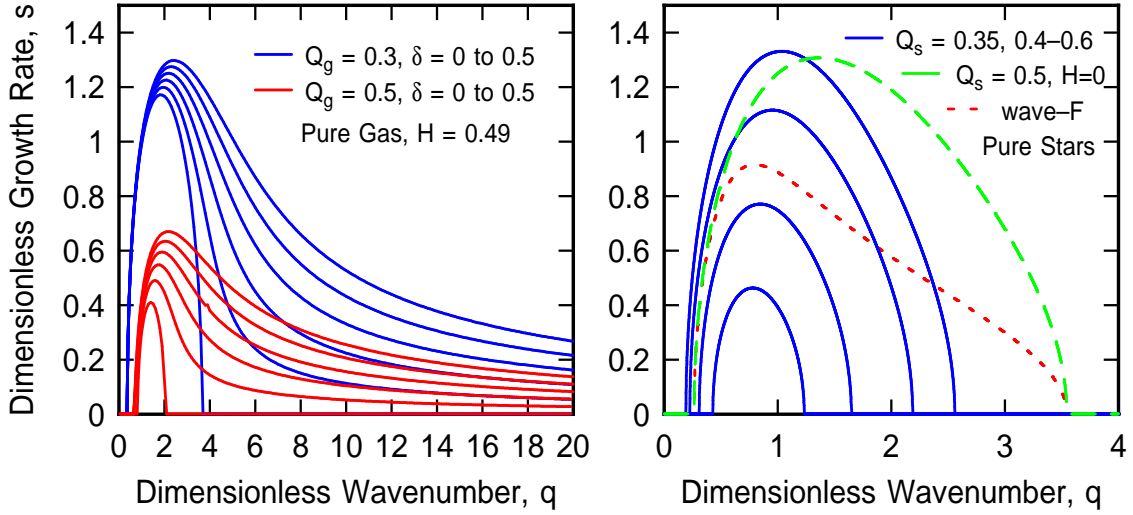


Fig. 3.— Solutions to the dispersion relation between growth rate and wavenumber are shown for a pure gas disk on the left and a pure star disk on the right. The different curves of the same type and color in the left panel are for different dimensionless dissipation rates. High dissipation leads to greater instability at high wavenumber. On the right, the four blue curves correspond to four values of Q_s including thickness corrections. The dashed green curve is for a zero thickness disk. The dotted red curve is a solution for a zero-thickness disk that uses a reduction factor \mathcal{F} evaluated in the case where the dispersion relation is oscillatory; such oscillations are unphysical for the assumed low Q_s , because these would give growth solutions. In comparison to the dashed green curve, the dotted red curve shows the importance of using the appropriate expression for the reduction factor.

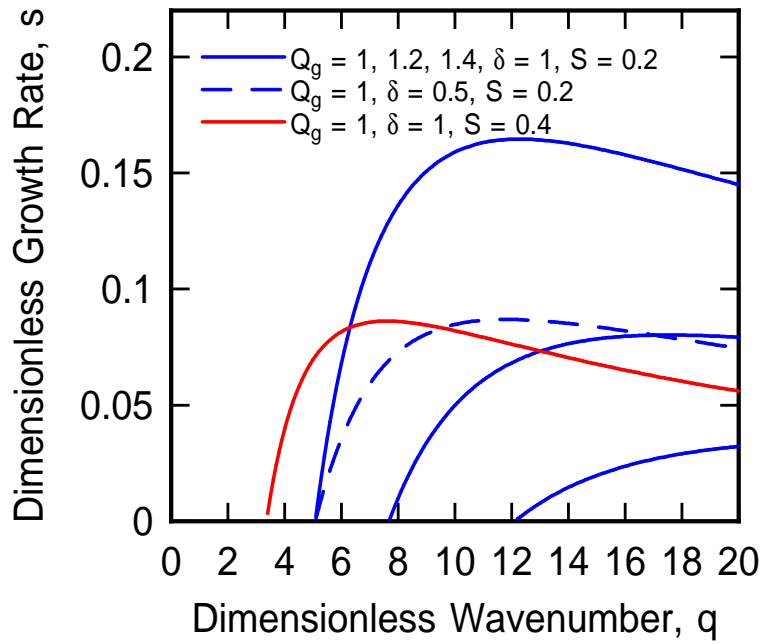


Fig. 4.— Dispersion relations for pure gas disks are shown in cases formerly thought to be stable, $Q_g \geq 1$. The destabilizing effect of the dissipation term involving δ can be seen. Thickness effects are included, and the stability at low q is from the dilution of in-plane self-gravity by disk thickness.

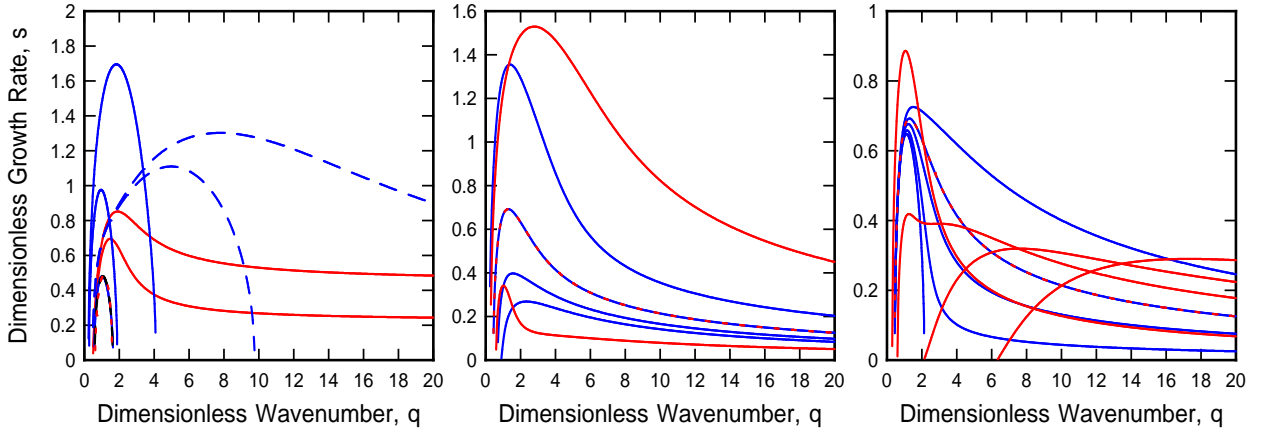


Fig. 5.— Solutions to the combined gas+star dispersion relation are shown. The left hand panel has several two-component cases that are effectively one-component, as a check on the equations. The dashed blue curves are two-component with $Q_s = 1$, $Q_g = 0.5$, and $S = 0.5$, and with dissipation parameter $\delta = 0.5$ on the top and $\delta = 0$ on the bottom. The middle panel shows a range of values for Q_s and Q_g at fixed $S = 0.5$ and $\delta = 0.5$. The sequence of blue curves with decreasing height has $Q_s = 0.5, 1, 1.5,$ and 2 for $Q_g = 1$, and the sequence of red curves with decreasing height has $Q_g = 0.5, 1,$ and 1.5 for $Q_s = 1$. The right hand panel shows the effect of dissipation as a sequence of blue curves ($\delta = 0, 0.1, 0.3, 0.5,$ and 1 with $S = 0.5$ from bottom to top) and the effect of the velocity dispersion ratio as a sequence of red curves ($S = 0.1, 0.2, 0.3, 0.5,$ and 1 with $\delta = 0.5$ from right to left). On the right, all have $Q_s = Q_g = 1$.

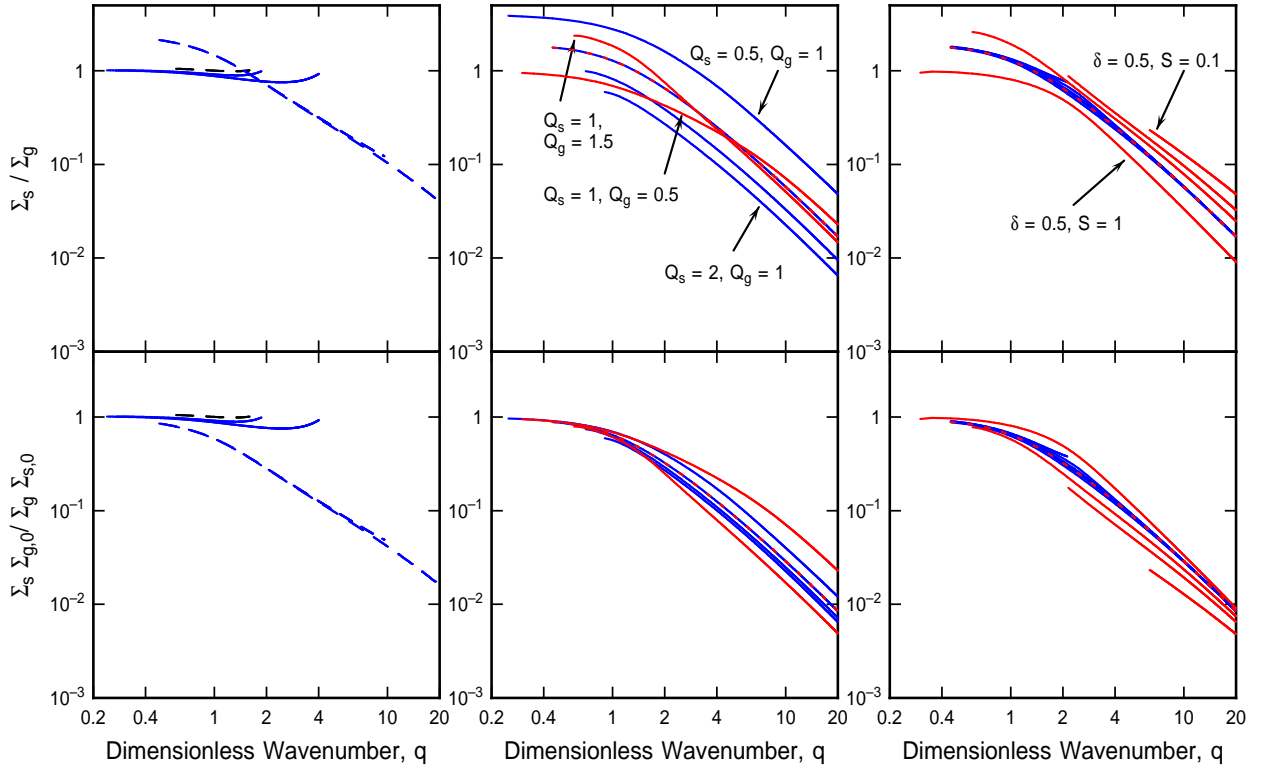


Fig. 6.— The ratio of perturbed stars to gas (top) and this same ratio normalized to the initial star-to-gas ratio (bottom) are shown versus wavenumber. The order of the panels, left to right, and the curve colors and types are the same as in Figure 7.

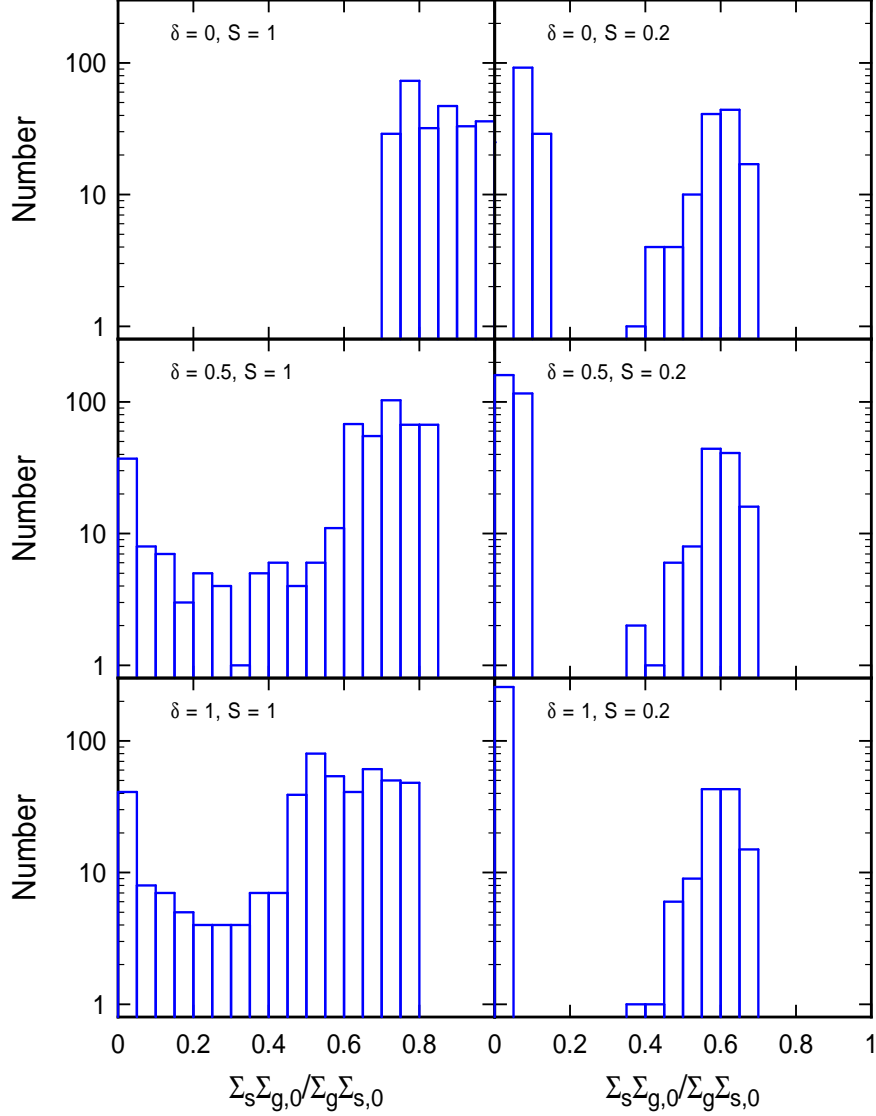


Fig. 7.— Histograms are shown of the normalize ratio of perturbed stars to gas at the wavenumber of peak growth. Each histogram is from a series of 800 cases with a range of Q_s and Q_g . Each panel has a different dissipation parameter and velocity dispersion ratio, as indicated. As dissipation increases in the high gas dispersion case (from top to bottom on the left), the gas plays a more prominent role in the growth of the instability (histograms shift to the left).

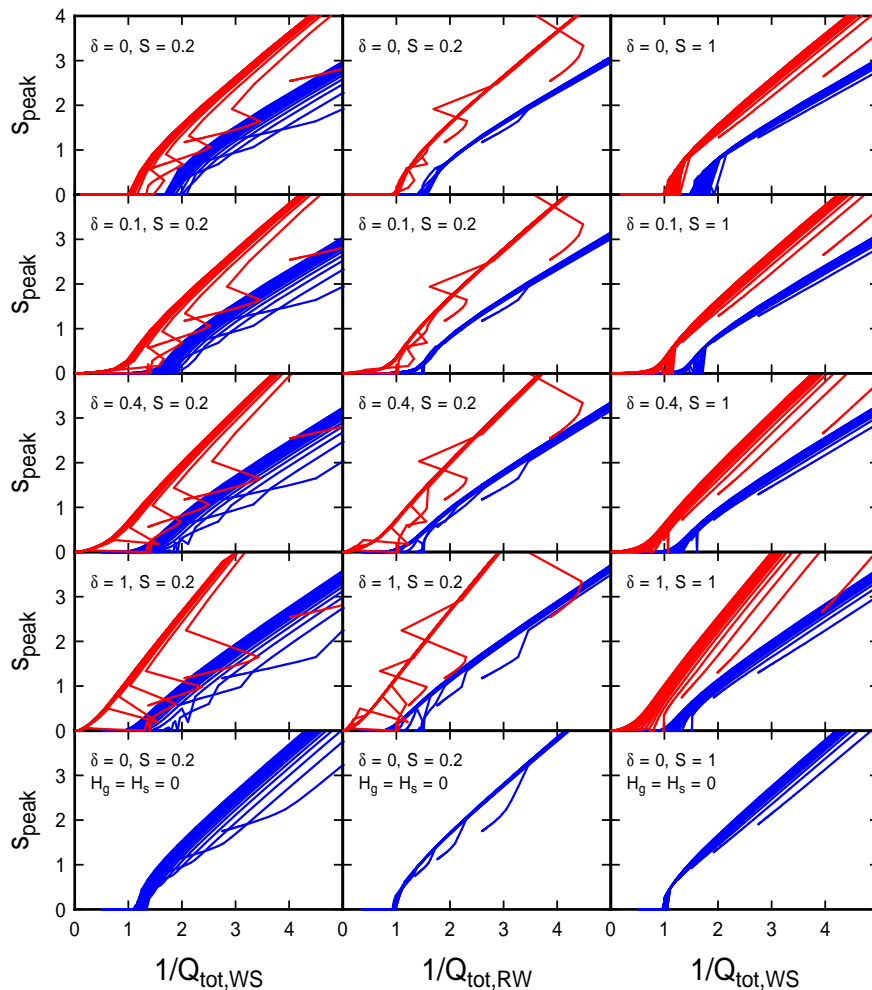


Fig. 8.— The peak growth rate of the gas+star dispersion relation is plotted as a function of $1/Q_{\text{tot}}$ for the Wang & Silk (1994) definition, on the left, and the Romeo & Wiegert (2011) definition in the middle. In these two cases, the velocity dispersion ratio is 0.2. On the right, the velocity dispersion ratio is unity and the two definitions of Q_{tot} are the same because the disk is effectively single-component. Each panel contains 20 blue curves and 20 red curves. Within each curve, Q_g varies, while the different curves are for different Q_s . In the top four rows, blue curves use an expression for Q_{tot} in which thickness effects are not considered, even though they are considered in the dispersion relation; red curves use expressions for Q_{tot} that include thickness corrections, and are therefore self-consistent. The top four panels differ in their value of the dissipation parameter δ . The bottom row solves the dispersion relation for a disk with zero thickness, which makes the red curves the same as the blue curves. The top four rows show how increasing dissipation always lowers $1/Q_{\text{tot}}$ at the threshold for instability, $s_{\text{peak}} = 0$.

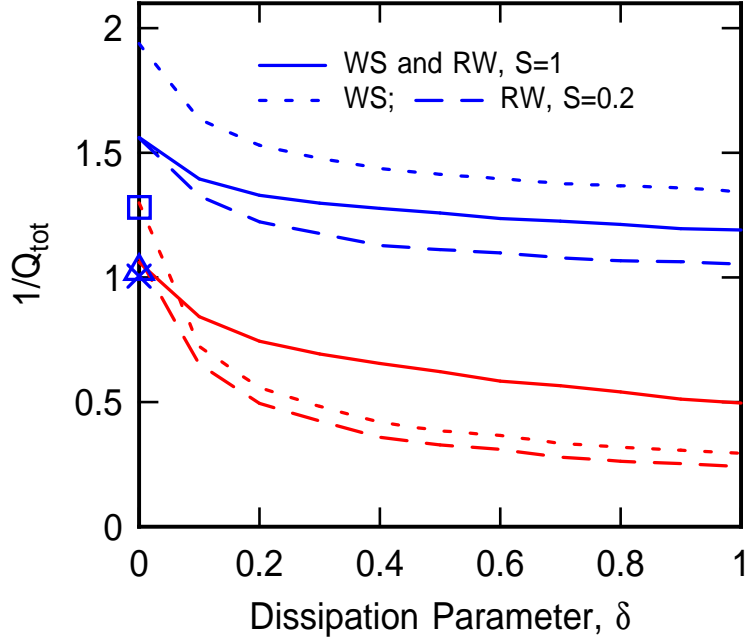


Fig. 9.— These curves plot the average values of $1/Q_{\text{tot}}$ where the peak growth rate, s_{peak} , is between 0.03 and 0.3, from Figure 10. These are essentially the stability thresholds for the various definitions of Q_{tot} . Blue curves ignore thickness corrections in the definition of Q_{tot} , as in Figure 10, while red curves explicitly account for thickness in Q_{tot} (all curves have thickness corrections in the actual dispersion relation). The three symbols on the ordinate axis are cases with zero-thickness disks. Dissipation lowers $1/Q_{\text{tot}}$ in all cases. For reasonable values of the parameters, Q_{tot} has to exceed 2 or 3 for a dissipative disk to become stable, instead of the usual threshold of ~ 1 .

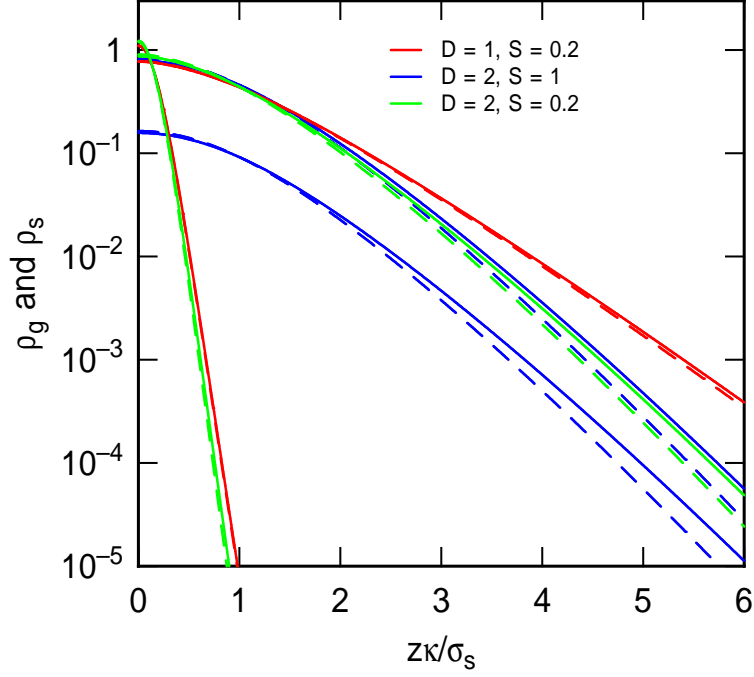


Fig. 10.— Vertical profiles for gas (quickly falling curves) and stars for two values of the dimensionless dark-matter parameter D (defined above equation A10) and two values of the ratio of gaseous to stellar velocity dispersion, S . The abscissa is the dimensionless height above the midplane. Solid curves are for a steep rotation curve, $\alpha = 0.4$, and dashed curves are for a nearly flat rotation curve, $\alpha = 0.04$ (defined below equation A8). Density is normalized to $\kappa^2 / (2\pi G Q_s)$ (see equations A11 and A12). These solutions assume $Q_s = 2$, $\hat{v}_{\text{rot}} = 8$, and $\Sigma_{g,0} / \Sigma_{s,0} = 0.2$.

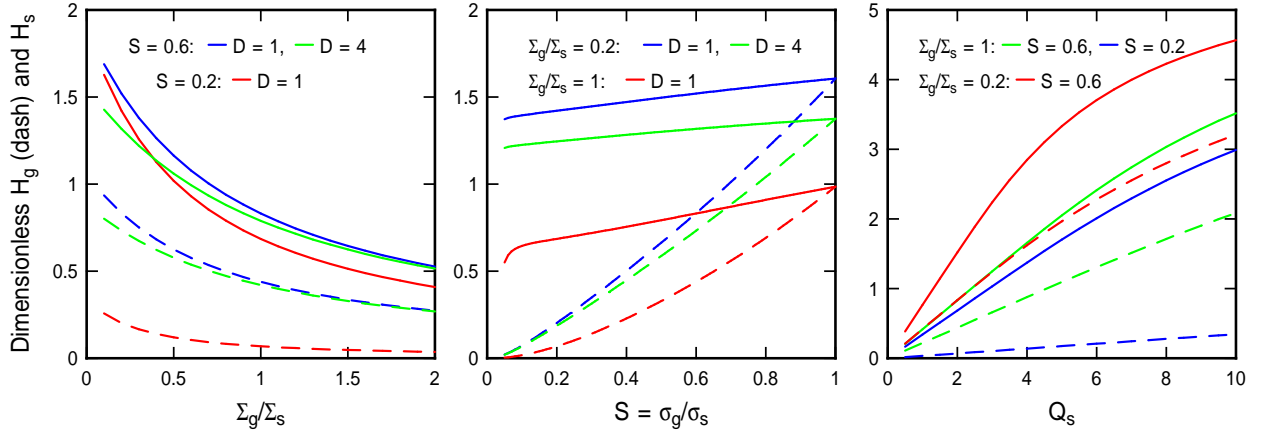


Fig. 11.— Dimensionless scale heights are plotted versus the gas fraction in the disk on the left, versus the gas-to-star velocity dispersion ratio in the middle, and versus Q_s on the right. Parameters associated with the various colors are indicated at the top of each panel. In the left and middle panels, $Q_s = 2$.

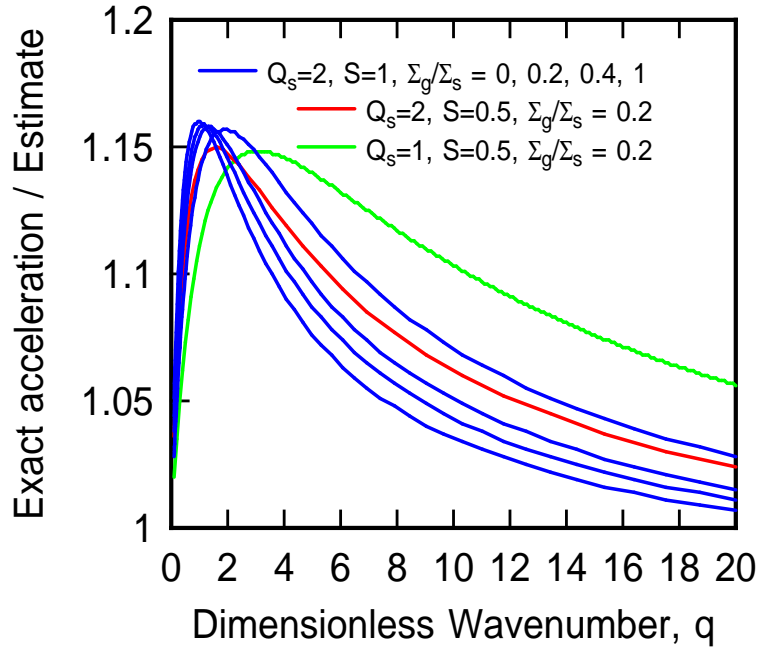


Fig. 12.— The curves show the correction factors for the in-plane acceleration in a thick disk compared to the approximate value using the term $(1 + kH)$. The correction factor for the growth rate is approximately equal to the square root of these acceleration factors. The correction factors are small, indicating that the usual approximation for disk thickness is good.